



A multi-objective benchmark for UAV path planning with baseline results

Daison Darlan ^a, Oladayo S. Ajani ^a, Anand Paul ^b Rammohan Mallipeddi ^a,*

^a Department of Artificial Intelligence, Kyungpook National University, Daehak-ro, Buk-gu, Daegu, 41566, South Korea

^b Biostatistics and Data Science Department, Louisiana State University, Health Sciences Center, New Orleans, 70112, LA, USA

ARTICLE INFO

Dataset link: <https://github.com/Anomaly33/UAV-Path-Planning-Benchmark>

Keywords:

UAV path planning

Multi-objective optimization

Autonomous navigation

ABSTRACT

Unmanned Aerial Vehicles (UAVs) are increasingly deployed in complex environments for applications such as urban logistics, surveillance, and environmental monitoring. Path planning for UAVs in these settings is a multi-objective optimization problem that must balance conflicting criteria such as safety, efficiency, and regulatory compliance. While heuristic methods like A* and Rapidly-Exploring Random Tree (RRT) have been applied to this problem, they often struggle with convergence speed and solution quality in obstacle-rich, three-dimensional spaces. Multi-Objective Evolutionary Algorithms (MOEAs) have shown strong potential for tackling such challenges, yet the absence of a comprehensive, standardized benchmark for UAV path planning continues to impede meaningful evaluation and comparison across studies. To address this gap, this paper makes three key contributions: (i) a parameterized framework for generating UAV path-planning problems across three representative environment types — urban, suburban, and mountainous — with adjustable scenario difficulty and real-world constraints such as no-fly zones; (ii) a curated benchmark suite comprising 14 diverse and rigorously designed test problems for reproducible and consistent algorithm evaluation; and (iii) baseline performance results for several state-of-the-art MOEAs, offering researchers clear reference points for future comparisons. By providing both a versatile testbed and a standardized evaluation methodology, this work aims to facilitate the development and fair assessment of UAV path-planning algorithms in realistic and challenging environments.

1. Introduction

Unmanned Aerial Vehicles (UAVs) have become indispensable in modern applications such as surveillance [1,2], delivery [3,4], and environmental monitoring [5]. UAV path planning involves determining an optimal or near-optimal route from a starting point to a destination, while optimizing key objectives under physical constraints. Traditionally, UAV path planning has been approached as a single-objective problem, where the primary focus was minimizing time or distance to the destination [6]. However, the increasing complexity of real-world UAV operations has rendered single-objective approaches impractical, as they fail to address the multi-faceted challenges inherent in UAV missions. In real-world scenarios, UAV path planning involves balancing multiple conflicting objectives, including travel time, energy consumption, and operational costs, while ensuring safety, obstacle avoidance, and compliance with regulatory restrictions such as altitude limits and no-fly zones. For instance, when planning a delivery route over a densely packed urban area, the UAV path must not only minimize travel time but also avoid obstacles like buildings. Moreover, additional constraints such as altitude limits and no-fly zones often

imposed in cities must be adhered to. In this context, if safety and flight-cost are selected as the objectives, they naturally conflict. Ensuring a safe flight may require the UAV to travel a longer, less direct route to maintain adequate safety margins in the presence of obstacles. Conversely, prioritizing flight-cost might compel the UAV to take a more direct path, which could increase the risk of collision. These conflicting objectives highlight the complexity and trade-offs inherent in UAV path planning, making multi-objective approaches increasingly relevant for real-world applications.

The quality of the generated path in UAV path-planning problems can be measured through various objective functions, depending on the specific application at hand. For instance, in a multi-drone network connectivity problem, it is crucial to ensure that individual drones remain within a specified distance from each other to prevent signal loss while simultaneously maintaining sufficient separation to maximize network coverage. Achieving this balance becomes particularly challenging in a pre-defined environment. Similar trade-offs can be observed across other UAV applications, where the path-planning objectives vary but share a common dependency on the environment's complexity. After

* Corresponding author.

E-mail addresses: daisondarlan33@gmail.com (D. Darlan), oladayosolomon@gmail.com (O.S. Ajani), apaul4@lsuhsc.edu (A. Paul), mallipeddi.ram@gmail.com (R. Mallipeddi).

thoroughly reviewing the literature, it becomes evident that regardless of the specific objective functions employed, the underlying complexity of path-planning problems can often be attributed to the design of the environment in which they are solved.

However, despite the growing importance of UAVs and their diverse applications, there remains no universally accepted benchmark for evaluating path-planning algorithms in complex three-dimensional environments. Researchers frequently design their own problem sets and environments, resulting in fragmented evaluations and inconsistent findings across different studies [7–11]. The absence of standardization significantly limits meaningful comparison of algorithm performance and effectiveness of various algorithms, especially when tested under different environmental conditions. While some works attempt to approximate real-world conditions using geospatial datasets [12–14], these approaches often encounter significant challenges. In many cases, the datasets are not readily accessible or the associated code is not publicly available, thereby limiting reproducibility and hindering consistent benchmarking across studies. Ghambari et al. [15] and Rocha and Vivaldini [7]. Moreover, benchmarks derived from real-world data are typically confined to the specific regions that have been mapped, limiting their capacity to represent the full spectrum of environmental conditions encountered in UAV operations. This is particularly problematic for extreme environments — such as mountainous regions — where the detailed variations in terrain and obstacle distribution are essential for realistic path-planning scenarios. Mapping these extreme regions is not only costly and inefficient [16], but it also restricts researchers from easily obtaining or expanding datasets for such challenging scenarios. As a result, the generalizability of findings derived from such datasets is significantly reduced, and the research community lacks a cohesive set of baseline scenarios for rigorous, head-to-head algorithm comparisons. In contrast, when the mathematical models for environment generation are clearly defined, they offer a more robust and versatile alternative. Such models allow for the systematic generation of synthetic datasets that can be tailored to capture a wide range of conditions — including extreme scenarios — without the logistical and financial constraints associated with real-world mapping. This modeling approach reduces reliance on limited geospatial datasets and facilitates the creation of benchmark scenarios that are both reproducible and adaptable.

Another drawback of many existing benchmarks is that they employ overly simplistic or abstracted representations of real-world environments [7,15]. For example, many studies resort to terrain approximations using basic peak or hill functions that neglect critical details, such as irregular obstacle geometry, varied building structures, and complex terrain gradients [17–19]. This oversimplification leads to benchmark environments that underrepresent the true difficulty of UAV missions [20]. In reality, UAVs are required to navigate dense urban structures with multi-level obstacles, irregular building layouts, and stringent airspace regulations—factors that are often absent or inadequately modeled in existing synthetic benchmarks [21,22]. Moreover, the majority of these benchmarks tend to focus on single-objective formulations, or use loosely combined objectives that fail to capture the necessary trade-offs inherent in real-world UAV operations [21]. Critical performance metrics such as energy consumption, flight time, collision risk, and altitude management are often optimized in isolation rather than in tandem. As noted by Debnath et al. [8], evaluating path planners on benchmarks that exclude key objectives — such as building density, altitude limits, and regulatory no-fly zones — can lead to solutions that perform well in artificially constrained settings yet fail to generalize when faced with the multifaceted challenges of real-world scenarios. In such cases, an algorithm might produce a short or energy-efficient path under idealized conditions, but may not be capable of safely navigating the complex and cluttered airspace encountered in urban or mountainous environments [16].

As a result, existing path-planning algorithms often exhibit limited robustness and adaptability when deployed in diverse, real-world conditions [23]. For instance, an algorithm designed to navigate a sparse,

simplistic environment may underperform in dense, cluttered urban settings or mountainous regions with significant elevation changes. Several literature reviews emphasize that lack of a standard, multi-objective, high-fidelity benchmark hinders meaningful comparisons among algorithms—particularly regarding convergence properties, computational efficiency, and adaptability across different terrains [24]. Without common datasets and standardized evaluation protocols, progress remains fragmented, as improvements demonstrated in one study might not translate to another with a different problem formulation or environment design. A key factor contributing to this challenge is the inability of many existing benchmarks to provide a diverse range of problem instances with varying difficulty levels. Most frameworks only support a fixed set of predefined test cases, limiting the flexibility needed to adapt environmental complexity for different experimental needs. They often lack mechanisms to systematically control key environmental parameters, such as obstacle density, terrain roughness, building distribution, or the presence of dynamic constraints, which are essential for evaluating the generalizability of UAV path-planning algorithms. Consequently, these benchmarks fail to assess how well algorithms perform across a spectrum of real-world challenges. In contrast, our proposed benchmark introduces a parameterized environment generation framework that enables fine-grained control over these factors, allowing researchers to create customized variations of the same scenario—ranging from relatively simple layouts to highly complex and obstacle-dense environments. This capability, which has not been adequately addressed in prior benchmarks, ensures that algorithms can be evaluated under a more comprehensive set of conditions, better reflecting the diverse challenges encountered in real-world UAV operations.

To bridge these gaps, this paper presents the following key contributions, which advance the state of UAV path planning research:

- **A novel and flexible framework** for systematically generating UAV path-planning problems in three distinct types of environments — urban, suburban, and mountainous — each representing common real-world scenarios with varying complexity. The framework incorporates a parameterized environment generation system that provides fine-grained control over important environmental features, including building density and height distributions, terrain undulations, and the spatial arrangement and severity of topographical obstacles such as peaks and ridges. This parameterization enables the creation of scalable problem instances with controllable difficulty, making it possible to evaluate the robustness and adaptability of path-planning algorithms in both routine and highly challenging scenarios. Furthermore, the framework allows the seamless integration of operational constraints, such as altitude limits and regulatory no-fly zones, ensuring that the generated problems remain realistic and practically relevant for UAV deployment in safety-critical missions.
- **A curated and comprehensive test suite** composed of 14 diverse path-planning problems, each carefully designed to capture a broad spectrum of environmental and regulatory challenges. These scenarios reflect real-world complexities, including densely clustered obstacles, rugged terrain variations, and the presence of restricted airspace, which collectively introduce complex multi-objective trade-offs between safety, efficiency, and regulatory compliance. The test suite provides a unified and standardized platform that facilitates fair, consistent, and reproducible performance comparison across UAV path-planning algorithms. By addressing a long-standing gap in the field — the lack of a widely accepted benchmark — the proposed test suite aims to promote more meaningful comparisons and accelerate the development of more generalizable UAV navigation strategies.
- **Baseline performance evaluations** of several widely used and state-of-the-art Multi-Objective Evolutionary Algorithms (MOEAs) on the proposed benchmark, covering both Pareto-based and

decomposition-based approaches. These experiments not only establish clear reference points for future research but also offer valuable insights into the strengths, limitations, and behavior of existing algorithms when applied to UAV path-planning problems across a variety of realistic and complex scenarios. The presented baseline results are intended to assist future studies in contextualizing their proposed methods and contribute to fostering a more rigorous and transparent evaluation culture in the UAV path-planning community.

The remainder of this paper is organized as follows. A comprehensive background on UAV path planning, encompassing both single-objective and multi-objective methodologies, is presented in Section 2, alongside an in-depth analysis of the challenges posed by real-world environments. The proposed multi-objective UAV path-planning benchmark is introduced in Section 3, detailing the underlying framework, environment generation procedures, and test suite construction. Section 4 provides information on the environments included in the test suite and discusses the rationale for their selection. The experimental design and methodology, including algorithm choice and evaluation criteria, are outlined in Section 5. Results and discussions are presented in Section 6, highlighting hypervolume metrics, statistical analyses, and algorithmic performance across various scenarios. Finally, Section 7 concludes the paper by summarizing the key findings, addressing their implications for UAV path planning, and proposing avenues for future research.

2. Background

2.1. Multi-objective Optimization (MOO)

Multi-objective optimization (MOO) addresses problems involving multiple conflicting objectives. In contrast to single-objective optimization (SOO), where a unique optimal solution is identified by comparing objective function values, MOO often leads to a set of solutions rather than a single optimum. This stems from the inherent conflict between objectives, where improving one often leads to compromises in others.

A general mathematical formulation for MOO can be represented as follows:

$$\begin{aligned} \min / \max \quad & f_m(\mathbf{x}), \quad m = 1, 2, \dots, M \\ & x_i^{\text{lower}} \leq x_i \leq x_i^{\text{upper}}, \quad i = 1, 2, \dots, n \end{aligned} \quad (1)$$

Here, M denotes the number of objective functions given by $f_m(\mathbf{x})$. The decision variables, \mathbf{x} are bounded within upper and lower limits for each variable, x_i^{lower} and x_i^{upper} where n is the total number of decision variables.

In multi-objective problems (MOPs), it is often impossible to find the “best” or optimum solution that optimizes all the objectives simultaneously. This is because, due to the conflicting nature of objectives in the MOP, a solution that has the highest value for a certain objective will inevitably not have the best value for another objective. Instead, solutions are often evaluated based on the concept of dominance. A solution \mathbf{x}_1 is said to dominate another solution \mathbf{x}_2 if it is at least as good in all objectives and strictly better in at least one objective. Mathematically,

$$\forall m \in 1, 2, \dots, M, \quad f_m(\mathbf{x}_1) \leq f_m(\mathbf{x}_2), \quad (2)$$

and

$$\exists m \in 1, 2, \dots, M, \quad f_m(\mathbf{x}_1) < f_m(\mathbf{x}_2) \quad (3)$$

The set of non-dominated solutions forms the Pareto front, which represents the trade-offs between competing objectives. Users can select their preferred solution based on their needs and the relative importance of the objectives, choosing from the Pareto front rather than settling for a single optimum as in SOO.

2.2. Multi-objective UAV path planning

UAV path planning is a critical component of autonomous navigation, requiring the determination of optimal paths that enable UAVs to reach designated target locations while adhering to various mission constraints. These constraints often include obstacle avoidance, energy efficiency, and operational boundaries, all of which are essential for achieving successful mission outcomes. Formulated as an optimization problem, path planning typically seeks to minimize a cost function $f(\mathbf{x})$, where \mathbf{x} represents the set of potential paths. This is subject to constraints $g(\mathbf{x})$ that capture environmental and operational limitations. Such formulations accommodate diverse representations, ranging from grid-based models to continuous-space frameworks, and employ advanced techniques such as graph-based algorithms and the calculus of variations [25].

Multi-objective optimization extends this foundational framework by addressing multiple, often competing objectives simultaneously. This approach enables UAVs to balance diverse criteria such as path length, energy consumption, collision avoidance, and path smoothness [18, 26, 27]. Unlike single-objective methods, which typically prioritize one specific goal, multi-objective frameworks accommodate the complexity of real-world operations, where UAVs must navigate dynamic and uncertain environments. These challenges include not only completing missions efficiently but also managing risks such as adverse weather, dynamic obstacles, and restricted zones.

By leveraging Pareto-optimality, multi-objective approaches do not converge on a singular “best” solution but instead produce a Pareto front of optimal trade-offs. This allows UAV operators to select solutions that align best with specific mission requirements [28]. For instance, multi-objective methods have demonstrated robust real-time performance by enabling UAVs to autonomously adapt routes to avoid obstacles while minimizing energy consumption. This balance is particularly crucial for long-duration missions or operations with stringent resource constraints [11]. Moreover, these approaches can integrate environmental uncertainties, such as wind disturbances or time-varying obstacles, to recalibrate paths dynamically [29, 30].

To address the challenges of UAV path planning, a wide range of algorithms has been developed and evaluated in diverse scenarios. Evolutionary optimization is one such framework, offering substantial flexibility in balancing multiple objectives through iterative refinement of candidate solutions. For example, Ren et al. [26] employed a Crowd Distance NSGA-II to minimize UAV travel distance and maximize safety in urban environment. This work demonstrated the potential of genetic algorithms to generate diverse, efficient paths, providing a strong basis for applications in urban settings where UAVs often face multiple constraints. Building on evolutionary approaches, Qiu and Duan [31] developed a multi-objective pigeon-inspired algorithm for UAV flocking in obstacle-dense environments. The algorithm distinguishes between hard constraints, which must be met, and soft constraints, which are optimized. Individuals that violate hard constraints are regenerated within the search space. However, due to the complex constraints typical of real-world environments, this approach may struggle to consistently produce valid solutions.

Swarm intelligence methods, inspired by natural collective behaviors, have also been applied to UAV path planning. For instance, Zhen et al. [32] developed a multi-objective PSO algorithm to address path length, path smoothness and path safety in mountainous terrain. Tested in simulations with sparse rounded and ragged hills, the paths generated demonstrated sufficient robustness compared to NSGA-II. However, as with many swarm-based approaches, the model's scalability to highly dense or obstacle-filled areas could benefit from additional testing. In a related study, Yu et al. [33] introduced a PSO-based algorithm SDPSO developed for UAV path planning in hilly terrains. This work took into account the path length, path altitude, UAV flight characteristics, and safety constraints associated with the path quality to create a weighted sum fitness function. While promising, real-world

adaptations would need to account for more variable conditions than what was encountered during the simulation studies.

Reinforcement learning (RL)-based methods have also shown potential for path planning by enabling UAVs to learn and adjust in response to complex environments. Qu et al. [34] employed a novel reinforcement learning based gray wolf optimizer algorithm called RLGWO that, optimizing for fuel cost, path safety and path deviation in a 3D environment with cylindrical obstacles. Although this approach showed promise under simulated threats, further research may explore its adaptability across a broader range of environmental disturbances such as denser obstacle field flight constraints such as altitude limits. A similar study was conducted by Zhang et al. [35] where Q-learning was combined with quantum-behaved PSO to address path length, altitude and threat in a similar environment as that of Qu et al. [34] but with the addition of rugged hilly terrain. While their results demonstrated that the approach could effectively manage multi-modal collaboration of UAVs in a complex environment, the simulations were limited to a single environment, which raises concerns about the generalizability of the findings. For instance, if the terrain's elevation were significantly increased, such that the height of obstacles approached that of the terrain, it remains uncertain whether the proposed approach would maintain its effectiveness in such a scenario.

The diverse range of environments encountered in UAV path planning presents significant challenges in developing standardized evaluation methods. Many studies focus on specific scenarios, yet the lack of consistency in environmental setups makes it difficult to compare the performance of different algorithms. This results in advancements that are often limited to isolated environments, without comprehensive cross-environment testing. As a result, while improvements are made, these studies may not fully address the practical complexities UAVs encounter in real-world applications, where conditions vary significantly across different environments. Our proposed benchmark addresses these limitations by focusing on static obstacles across three distinct environments: urban, suburban, and mountainous. This approach ensures that the path planning algorithms are evaluated in scenarios with static, fixed obstacles, which are more common in many practical applications. In each environment, we emphasize different challenges. For instance, in a mountainous environment, we test the algorithm's ability to navigate areas with high mountains and no-fly zones, whereas in suburban settings, the algorithm must plan paths around less clustered obstacles but with restrictions on the proximity to no-fly zones. This strategy of algorithm evaluation ensures that UAV path planning algorithms are tested across a broad spectrum of realistic challenges, making it easier to compare and evaluate their performance in scenarios that closely mirror real-world applications. Ultimately, the benchmark aims to support the development of more adaptable algorithms that can be deployed in a variety of practical missions.

3. Proposed framework for UAV path planning problem generation

In this section, details regarding the construction of the benchmark are presented along with the characteristics of the 14 test problems. First, the mathematical modeling required to generate the environments is discussed, followed by the representation of the environment as well as the path. Although the solution representation is discussed from the perspective of the adopted methodology, it should be noted that the problems are developed as standalone systems capable of being adapted to any framework. The path evaluation criteria, by which the quality of the generated paths can be assessed, are then discussed, followed by an in-depth examination of the bounding constraints inherent to the framework.

3.1. Environment generation

In the context of UAV path planning, the generation of a realistic and computationally manageable environment is crucial for testing and optimizing algorithms. This section describes the methodology employed to create a synthetic environment that combines natural terrain features with urban-like structures such as buildings. The mathematical formulations used for the environment generation are based on established principles of terrain modeling, ensuring that they closely mimic natural features observed in urban, suburban and mountainous environments. A similar categorization strategy is used to explain the methodology for generating terrain and describe how they are suited to represent real-world scenarios.

3.1.1. Urban environment

Terrain undulations: Cities are typically characterized by flat or gently undulating terrain dominated by structures such as buildings and roads, often constructed on relatively level landscapes with minimal elevation changes. However, introducing small undulations in the terrain is valuable as it adds complexity to UAV path planning. Even slight variations in terrain elevation can influence UAV flight dynamics and impose subtle constraints, particularly in low-altitude operations [36]. While terrain-induced effects such as wind turbulence are not modeled in this study, undulations still challenge path-planning algorithms by introducing varying altitude constraints. Accordingly, terrain variations have been incorporated across all generated environments, with their magnitude and frequency tailored to the specific characteristics of each setting. For a high-rise city environment, the terrain undulations are created using sinusoidal functions represented as follows:

$$T_{\text{city}}(x, y) = A \sin\left(\frac{2\pi}{\lambda_x} x + \phi_x\right) + B \cos\left(\frac{2\pi}{\lambda_y} y + \phi_y\right) \quad (4)$$

Here, the variables A and B control the height of the undulations. Small values ($A, B < 1$) represent the generally flat terrain of cities, with minimal elevation changes. The wavelengths λ_x and λ_y modulate the slope of the sinusoidal waves, with longer wavelengths ($\lambda > 1$) creating gentle slopes that are suitable for flat urban areas. To introduce variability, phase shift parameters ϕ_x and ϕ_y are introduced, which offset the sinusoidal patterns, preventing regularity and allowing for the generation of more realistic terrain undulations.

Building placement: The complexity of a city environment primarily arises from the height and density of the buildings. A dense arrangement of buildings with significant variability in height is necessary to accurately simulate real-world conditions. Therefore, in this work, the buildings are modeled as cuboidal structures. The building density in the generated environment is controlled by the N_{bldg} parameter, which can be adjusted to simulate sparse or crowded cityscapes, respectively (Fig. 1). Furthermore, to introduce randomness in building heights, as observed in cities ranging from low-rise residential buildings to high-rise skyscrapers, the building heights are sampled from a uniform distribution as follows:

$$H_b \sim U(H_{\min}, H_{\max}) \quad (5)$$

where H_{\min} and H_{\max} correspond to the minimum and maximum allowable building heights, respectively. The introduction of this parameter in the environment generation process provides greater flexibility in the complexity of the environment required for trajectory planning. Finally, the city terrain with N_{bldg} buildings can be obtained as:

$$z_{\text{city}} = T_{\text{city}}(x, y) + \sum_{i=1}^{N_{\text{bldg}}} H_b(i) \quad (6)$$

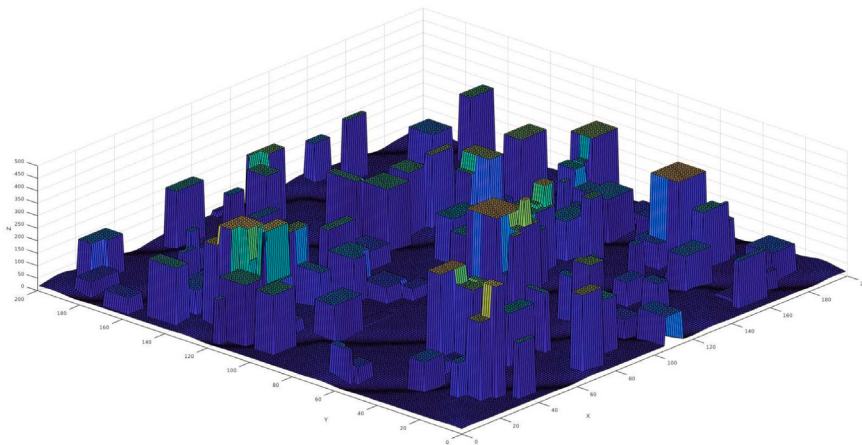


Fig. 1. A visualization of an urban environment with cuboid buildings and slight terrain undulations. Each grid square represents a unit in the environment, emphasizing the challenges of UAV navigation in densely constructed cityscapes.

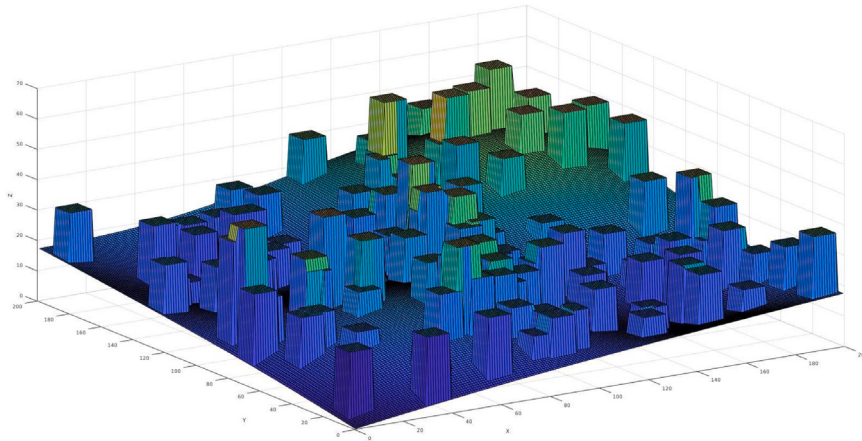


Fig. 2. A depiction of a suburban environment characterized by rolling hills of varying heights and scattered buildings. This environment reflects the transitional complexity between urban density and rural openness for UAV path planning.

3.1.2. Suburban environments

Suburban areas serve as transitional zones between urban and rural environments, characterized by a blend of hills and scattered buildings, although the density of buildings can also be high. In the suburban environment generated in this work, the main distinction from the city environment is the greater variation in altitude. This combination of altitude changes and the scattered distribution of buildings presents unique challenges not encountered in high-rise urban environments, where the UAV must navigate varying terrain gradients while avoiding obstacles.

Terrain undulations: Suburban terrain often features rolling hills and a random scattering of buildings. By combining multiple sinusoidal components with varying amplitudes and wavelengths, realistic undulations can be created to mimic the gentle slopes and varied topography typically found in suburban areas as depicted in Fig. 2. Mathematically, this can be expressed as:

$$T_{\text{suburb}}(x, y) = \sum_{i=1}^N A_i \sin\left(\frac{2\pi}{\lambda_i} x + \phi_{x,i}\right) + \sum_{j=1}^M B_j \sin\left(\frac{2\pi}{\lambda_j} y + \phi_{y,j}\right) \quad (7)$$

where the number of components (N, M) controls the number of sinusoidal waves generated, while A_i and B_j guide the height of each of the waves generated. Increasing the values of either of N or M increases the overlap of the sinusoidal waves, creating rougher and more realistic terrain.

Small hills and buildings: The small localized hills in suburban environments are represented by the following Gaussian function:

$$M_{\text{hill}}(x, y) = H_h \exp\left(-\frac{(x - x_h)^2}{2\sigma_x^2} - \frac{(y - y_h)^2}{2\sigma_y^2}\right) \quad (8)$$

Here, H_h represents the height of the hill where smaller values of H_h are used to create smaller but broader peaks. x_h and y_h in Eq. (8) represent the mean of the Gaussian curve, which translates to the center of the hill in the environment. The spread of hills in the x and y directions is performed using the parameters σ_x and σ_y . The higher value for these parameters generates broader and less steep hills commonly found in sub-urban areas.

The height of the terrain at any point in the environment can hence be calculated by combining Eqs. (7) and (8) as:

$$z_{\text{suburb}} = T_{\text{suburb}}(x, y) + M_{\text{hill}}(x, y) \quad (9)$$

3.1.3. Mountainous environment

Path planning in mountainous terrains poses significant challenges due to the inherent complexities of the environment. UAVs operating in such regions must navigate substantial elevation variations, steep gradients, and rugged surfaces to identify an optimal trajectory. In this work, the complexity of the terrain is modeled by increasing the number of sinusoidal components and their amplitudes compared to city and suburban environments.

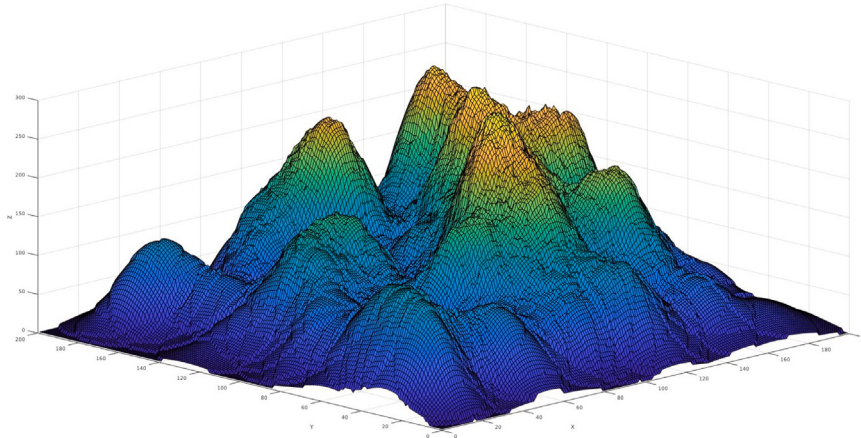


Fig. 3. A simulated mountainous terrain with multiple pronounced peaks, steep gradients, and significant altitude variations. This highlights the intricate path-planning challenges posed by rugged topographical features.

Additionally, multiple elevation peaks are introduced using a Gaussian-based representation to emulate the sharp variations characteristic of mountainous regions (Fig. 3). The terrain model is defined as:

$$M_{\text{mount}}(x, y) = \sum_{i=1}^{N_{\text{peaks}}} H_k(i) \exp\left(-\frac{(x - x_k)^2}{2\sigma_x^2} - \frac{(y - y_k)^2}{2\sigma_y^2}\right), \quad (10)$$

where N_{peaks} denotes the total number of peaks, and $H_k(i)$ specifies the height of the i th peak. The parameters σ_x and σ_y control the spread of each Gaussian component along the x and y axes, respectively. In comparison to suburban environments, H_k values are set significantly larger ($H_h \ll H_k$), while σ_x and σ_y are reduced to produce steeper and more pronounced elevations. Increasing N_{peaks} introduces overlapping peaks, thereby enhancing the terrain's overall complexity.

To simulate natural irregularities such as uneven ground, rock formations, and vegetation, a noise function is incorporated into the terrain model. The noise is represented as:

$$R_{\text{mount}}(x, y) = \gamma \cdot \mathcal{N}(0, \sigma_r^2), \quad (11)$$

where $R_{\text{mount}}(x, y)$ introduces random perturbations along the z -axis at each grid point (x, y) . These perturbations are modeled as Gaussian noise (\mathcal{N}) with a standard deviation σ_r , and their magnitude is scaled by a ruggedness factor γ . The final terrain elevation is computed by superimposing the Gaussian-based peaks with the noise function:

$$z_{\text{mount}}(x, y) = M_{\text{mount}}(x, y) + R_{\text{mount}}(x, y). \quad (12)$$

This methodology ensures the generation of realistic mountainous terrains featuring steep inclines, intersecting valleys, and multiple overlapping peaks. The added complexity challenges UAV path-planning algorithms by simulating a high-fidelity environment that closely resembles real-world conditions.

3.2. Path representation and smoothing

In the benchmark formulation, a grid-based representation is utilized for path definition. The environment is discretized into uniform grids of unit length ($\Delta x, \Delta y, \Delta z$), creating a structured spatial framework. Each grid point is represented by its coordinates (x_i, y_i, z_i) , enabling precise localization of the UAV in 3D space. Consequently, a path P is expressed as a sequence of N grid points as:

$$P = \{(x_1, y_1, z_1), (x_2, y_2, z_2), \dots, (x_N, y_N, z_N)\} \quad (13)$$

As discussed, the path of a UAV is defined by a series of waypoints, which are decision variables in the planning process. To ensure smooth navigation, path-smoothing techniques are applied, converting discrete

waypoints into a continuous trajectory. The B-spline method is frequently chosen for this purpose due to its efficiency and versatility in creating smooth paths, making it ideal for UAV path planning [37–39]. Given the discrete path representation $P = \{(x_i, y_i, z_i)\}_{i=1}^N$, a B-spline is utilized to interpolate these points and generate a continuous trajectory. The smoothness of the path generated depends upon the degree of the B-spline curve. A higher degree results in a smoother curve with greater flexibility in fitting complex paths, but it also increases computational complexity. A B-spline curve of degree d is defined as:

$$C(u) = \sum_{i=0}^m \mathbf{P}_i N_{i,d}(u), \quad u \in [0, 1] \quad (14)$$

where \mathbf{P}_i are the control points, $N_{i,d}(u)$ are the B-spline basis functions, and m is the total number of control points minus 1. Increasing the number of control points, \mathbf{P}_i enhances its flexibility and allows for more precise shaping, as each additional control point provides greater local influence over the curve's form. However, this increase also introduces complexity in managing and adjusting the control points, which can complicate the design process [40]. The basis functions $N_{i,d}(u)$ determine how much influence each control point \mathbf{P}_i has on the B-spline curve at any given value of u . Essentially, they assign a weight to each control point based on the parameter u and its corresponding knot values. The basis functions are recursively computed using:

$$N_{i,0}(u) = \begin{cases} 1, & t_i \leq u < t_{i+1} \\ 0, & \text{otherwise,} \end{cases} \quad (15)$$

$$N_{i,d}(u) = \frac{u - t_i}{t_{i+1} - t_i} N_{i,d-1}(u) + \frac{t_{i+d+1} - u}{t_{i+d+1} - t_{i+1}} N_{i+1,d-1}(u) \quad (16)$$

where, t_i are the knot values define the partitioning of the parameter domain $[0, 1]$. They specify the intervals over which each control point \mathbf{P}_i has influence on the curve. The placement and distribution of the knots determine how the curve is shaped, affecting its continuity and smoothness. A uniform knot vector results in evenly spaced influence, while non-uniform knots can introduce varying control over the curve's behavior, making it more flexible or constrained depending on the application. In this work, uniform knots as depicted in Fig. 4 are used for the B-spline formulation due to its simplicity and computational efficiency.

3.3. Path evaluation

To evaluate the quality of a planned UAV path, various criteria are considered based on the specific application. The most commonly used evaluation functions include path length, flight duration, flight height, and energy consumption. However, in many cases, flight duration can be treated as a function of path length. Explicitly modeling energy

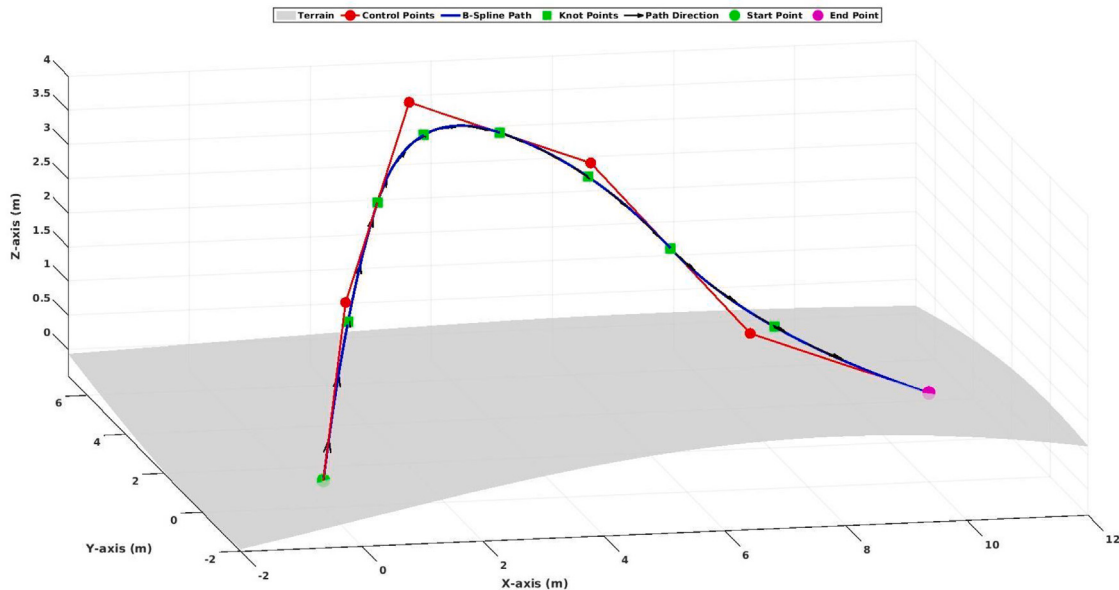


Fig. 4. 3D UAV path planning using a B-spline curve. The smooth path (blue) is guided by control points (red), with knot points (green) and trajectory direction indicated by black arrows.

consumption often introduces unnecessary complexity, as path length and altitude provide efficient proxies for energy usage. Horizontal energy consumption is strongly correlated with path length, as drag forces are influenced by the path distance and UAV speed. Similarly, altitude directly impacts lift and air density, which govern energy usage during hovering or climbing. The total energy consumption can be approximated as:

$$E_{\text{approx}} = k_L L + k_H H \quad (17)$$

where k_L and k_H are environment and UAV-specific scaling factors for path length (L) and flight height (H), respectively. Therefore, by optimizing L and H , the computational overhead can be minimized while maintaining a strong correlation with actual energy consumption.

The objective of minimizing path length is to reduce the total distance the UAV must travel between waypoints, thereby ensuring an efficient route. Mathematically, the path length L for a path with N waypoints is computed as the sum of Euclidean distances between consecutive waypoints:

$$L = \sum_{i=1}^{N-1} \sqrt{(x_{i+1} - x_i)^2 + (y_{i+1} - y_i)^2 + (z_{i+1} - z_i)^2} \quad (18)$$

For flight height, the objective is to minimize altitude variations to ensure the UAV operates within a specific flight envelope, enhancing energy efficiency and safety. The average flight height H_{avg} is calculated as the mean of the altitudes z_i at each waypoint:

$$H_{\text{avg}} = \frac{1}{N} \sum_{i=1}^N z_i \quad (19)$$

By minimizing path length and optimizing flight height, UAVs can achieve more efficient and safer flight paths. Furthermore, path length optimization is directly related to energy consumption models, as shorter paths generally result in reduced energy usage. Minimizing altitude variations ensures that the UAV remains within optimal operating ranges, minimizing unnecessary altitude changes that could lead to energy inefficiencies.

3.4. Constraints

In the UAV path planning framework, several constraints ensure safe and efficient flight across different environments. A critical constraint

in urban environments is the maximum allowable flight height, which prevents the UAV from colliding with tall buildings or exceeding regulatory restrictions. This constraint can be expressed mathematically as:

$$z_i \leq h_{\max}^{\text{UAV}}, \forall i \in [1, 2, \dots, N], \quad (20)$$

where z_i is the flight height at waypoint i and h_{\max}^{UAV} is the maximum allowable flight height for the UAV. In this study, h_{\max}^{UAV} is set to 120 units, representing a typical operational ceiling that complies with both urban regulations and the UAV's flight capabilities. Similarly, a minimum height limit is set for the UAV in all terrains to maintain a safe operating height away from the terrain and obstacles. This constraint is defined as:

$$z_i \geq h_i^{\text{terrain}} + h_{\text{safe}}. \quad (21)$$

Here, h_i^{terrain} corresponds to the height of the terrain at waypoint i , and h_{safe} represents the safe height constant, which is set to 5 units in this study to ensure adequate clearance from obstacles. In the context of UAV operations, these constraints represent bound constraints from an evolutionary algorithms perspective, ensuring that the search space for optimal solutions is well-defined and feasible. In this study, constraints are primarily enforced through the problem formulation. New solutions are validated for compliance upon generation, and only those that satisfy all constraints remain in the population. While alternative approaches can integrate constraint handling within the algorithm itself, a formulation-centric strategy is adopted to maintain a straightforward mapping between real-world restrictions and the search space. This approach confines the optimization process to feasible trajectories without complicating the algorithmic implementation.

Turning angle constraints are fundamental operational limits that ensure the vehicle's trajectory remains feasible within its physical and aerodynamic capabilities. These constraints are imposed on both horizontal and vertical turning angles to prevent abrupt directional changes that could compromise stability, efficiency, or structural integrity. The horizontal turning angle constraint θ_h defines the maximum allowable change in direction between consecutive waypoints in the x - y plane, while the vertical turning angle constraint θ_v limits the variation in altitude along the z -axis relative to the horizontal plane. Mathematically, the horizontal turning angle is expressed as:

$$\theta_h = \arccos \left(\frac{v_i \cdot v_{i-1}}{|v_i| |v_{i-1}|} \right), \quad (22)$$

Table 1

A comprehensive list of parameters used to configure UAV path-planning scenarios. These parameters include environmental attributes (e.g., building height and density, mountain peak characteristics) and operational constraints (e.g., flight height limits, no-fly zone specifications), enabling tailored problem setups for benchmarking algorithms across diverse environments.

Parameters	Definition
$h_{\text{max}}^{\text{bldg}}$	Maximum height of the buildings
N_{bldg}	Number of building
A_{search}	Size of the search space
$w_{\text{min}}^{\text{bldg}}$	Minimum building width
$w_{\text{max}}^{\text{bldg}}$	Max building width
$h_{\text{max}}^{\text{UAV}}$	Maximum allowable flight-height
θ_h^{max}	Maximum horizontal turning angle
θ_v^{max}	Maximum vertical turning angle
Δh_{max}	Amplification factor for altitude variations
r_{NFZ}	Radius of the no-fly-zone
h_{NFZ}	Ceiling of the no-fly-zone
\mathbf{p}_{NFZ}	No-fly-zone position vector
N_{peaks}	Number of mountain peaks
$h_{\text{max}}^{\text{peaks}}$	Maximum height of mountain peaks

where $v_i = (x_{i+1} - x_i, y_{i+1} - y_i)$ is the horizontal vector, and $|v_i|$ is the norm of the vector defining two consecutive path segments. In this study, the maximum horizontal turning angle θ_h^{max} is set to 45 degrees, ensuring smooth directional changes. Similarly, the vertical turning angle is expressed as:

$$\theta_v = \arccos \left(\frac{\mathbf{u}_i \cdot \mathbf{u}_{i-1}}{|\mathbf{u}_i| |\mathbf{u}_{i-1}|} \right), \quad (23)$$

where $\mathbf{u}_i = (x_{i+1} - x_i, y_{i+1} - y_i, z_{i+1} - z_i)$ is the 3D vector between two waypoints. The maximum vertical turning angle θ_v^{max} is similarly constrained to 30 degrees, ensuring safe altitude variations.

The selection of these maximum turning angle values is influenced by the UAV's dynamic constraints, particularly the maximum turning radius defined by the maximum roll angle and ground speed [41]. Additionally, studies have shown that within the maximum turning angle limit, smaller turning angles contribute to smoother flight trajectories [42], though they may affect maneuverability. Therefore, setting θ_h^{max} to 45 degrees and θ_v^{max} to 30 degrees balances the need for smooth trajectory changes with the UAV's maneuverability and structural integrity.

The impact of No-Fly Zones (NFZs) on UAV path planning has been extensively studied in aerospace applications. Avoidance of NFZs often necessitates significant detours, which can conflict with key optimization objectives such as minimizing flight time, energy consumption, or total travel distance. These trade-offs are typically more pronounced compared to static physical obstacles, such as buildings, where the detours are relatively smaller. In this study, the environment is modeled to include NFZs that are circular in shape with variable heights. The height of each NFZ is set to be 30 units greater than the tallest peak or building within its vicinity to ensure complete avoidance of restricted airspace. Additionally, the NFZs are assumed to be temporally invariant in both size and location, simplifying the planning process while maintaining realism.

4. Multi-objective UAV path planning test suite

To illustrate the characteristics and capabilities of the proposed benchmark, a test suite consisting of 14 problems has been generated. Each problem has been carefully crafted with parameters thoughtfully selected to ensure that it poses a unique challenge to the path planning process. The naming scheme for the test suite is designed to provide a concise yet descriptive representation of the adjustable parameters for each test problem across the three environments: urban, suburban, and mountainous. Each problem is named using the

format [Environment]_[Type]_[KeyParams], where the environment is represented by a single letter (C for city/urban, S for suburban, and M for mountainous), followed by a sequential identifier for the problem type (e.g., 01, 02), and a set of abbreviated key parameters. The key parameters encode critical attributes, such as the number of buildings or peaks (N), maximum height (H), no-fly-zone radius (R), and no-fly-zone position (P). For example, the name M02_N8_H70_R40_P20,30 represents a mountainous environment (M), the second problem in that category (02), with 8 peaks (N8), a maximum peak height of 70 (H70), a no-fly-zone radius of 40 (R40), and a no-fly-zone positioned at coordinates (20, 30). This scheme ensures consistency across all test cases, provides sufficient detail to differentiate between problems, and maintains brevity for clarity in reporting and analysis.

4.1. High rise city

For the urban environment, four distinct test cases as shown in Fig. 5 have been developed, each designed to evaluate specific challenges in UAV path planning. Among these, two cases do not include no-fly zones, allowing the focus to remain on navigating building-dense cityscapes. Following the naming convention, these test cases are designated as C01_N100_H450 (C1) and C02_N150_H450 (C2). The primary difference between these two test cases lies in the density of buildings: C1 represents a typical urban environment with 100 buildings, while C2 simulates an exceptionally dense city with 150 buildings. This variation enables testing the algorithm's ability to adapt to both moderately constrained environments and highly congested urban landscapes where maneuvering through tight spaces becomes critical. The adjustable environment parameters are presented in Table 1. In our design, test cases C1 and C2 are ideally tailored for urban surveillance. This is evidenced by Muñoz et al. [43], who introduced a leader-follower strategy for cooperative persistent surveillance in unfamiliar urban areas, and by Zhou et al. [44], who tackled urban monitoring with UAVs by formulating it as a mixed-integer quadratically constrained problem. Both studies addressed the challenge of maintaining UAV connectivity in cluttered city environments—precisely the issues that the developed problems target.

Additionally, two urban test cases incorporate no-fly zones to introduce additional navigational constraints. These are labeled as C03_N10_0_H450_R20_P100, 100 (C3) and C04_N70_H450_R40_P100, 100 (C4). C3 features a dense cityscape with 100 buildings and a relatively small no-fly zone of radius 20 centered at (100, 100), making it ideal for testing urban search and rescue (SAR) applications—where rapid route planning around compact, restricted regions is critical, as illustrated by Erdelj et al. [45] and Chowdhury et al. [46]. In contrast, C4 presents a sparser urban environment with 70 buildings and a larger no-fly zone of radius 40, which is well suited for urban logistics tasks such as drone delivery. In this context, route optimization and risk-aware planning become essential; Song et al. [47] formulated a MILP for multi-stop route optimization in dense urban settings, while Kim et al. [48] introduced a cost-benefit model that assigns risk costs for flying over rooftops and roads, yielding safer delivery paths that are only marginally longer than those from basic A* plans. Finally, these scenarios also support urban infrastructure inspection tasks. For instance, Zheng et al. [49] utilized a virtual reality-based planning system to simulate building facade inspection in high-density urban areas, and real-world trials have demonstrated that UAVs can effectively conduct bridge and tower inspections by autonomously orbiting structures with high-resolution cameras.

Together, these test case closely mimics the dense, structured nature of modern cities. The terrain is modeled with subtle sinusoidal undulations that simulate the slight elevation differences commonly found in urban landscapes, while a randomized placement of cuboid buildings with varying heights reflects the diverse architectural structures encountered in metropolitan areas. This design not only captures the

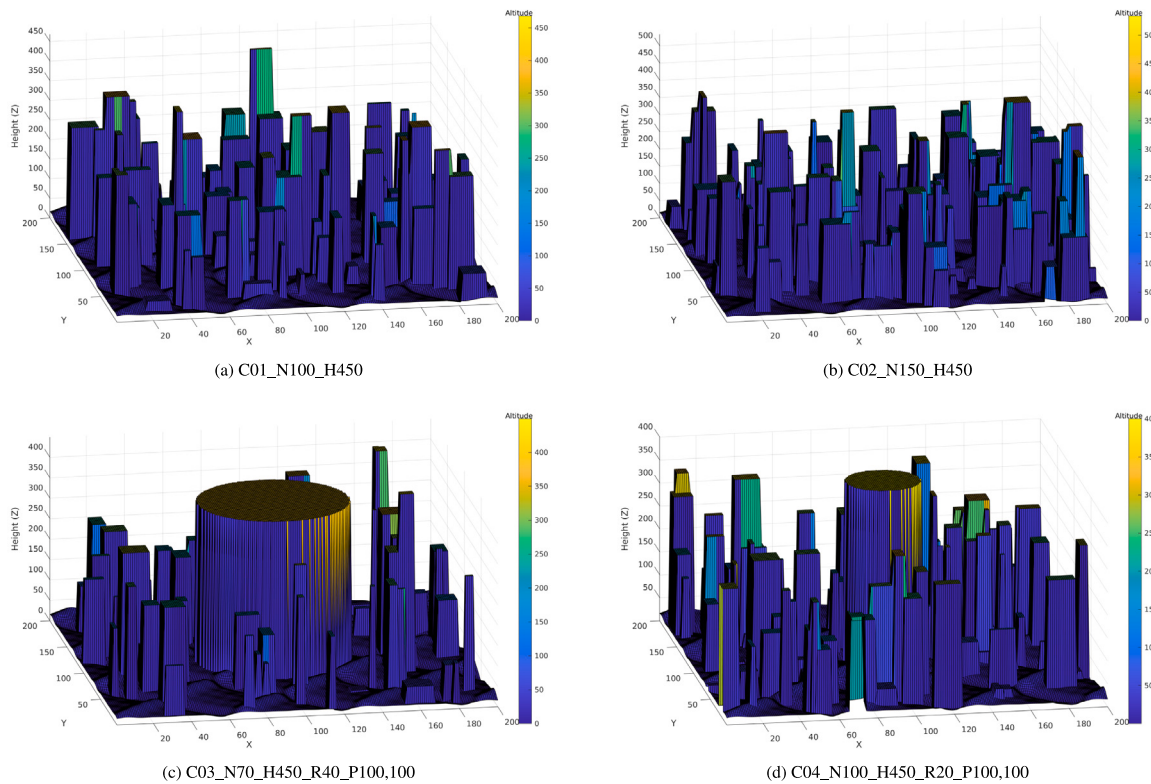


Fig. 5. Visual representations of urban test cases with varying building densities and the presence or absence of no-fly zones. Each scenario evaluates UAV path-planning performance in dense cityscapes with specific constraints such as building layouts and restricted flight zones.

physical complexity — such as narrow corridors and clustered obstacles — but also integrates regulatory constraints by incorporating no-fly zones and altitude restrictions, thereby replicating the legal and safety requirements imposed in urban airspaces [50]. Such detailed modeling is crucial, as drones in cities must navigate through densely built areas and adhere to strict flight regulations.

4.2. Suburban

For the suburban environment, four distinct scenarios (Fig. 6) have been constructed to examine the challenges of UAV path planning in moderately built areas with varying levels of complexity. Two scenarios do not include no-fly zones, enabling a focused assessment of path planning in environments with varying building densities. These scenarios are designated as S01_N120_H40 (S1) and S02_N180_H40 (S2), where S1 represents a standard suburban setting with 120 medium-height buildings and S2 simulates a more congested layout with 180 buildings. These cases are particularly suited for suburban surveillance tasks, as evidenced by Szczepański [51], who discussed the problem of detecting pollution emission sources in a low buildings area using UAVs. In addition to surveillance, these scenarios are also applicable for last-mile delivery [52] where drones can reliably navigate suburban landscapes to deliver packages.

The remaining two scenarios, S03_N80_H40_R40_P100,100 (S3) and S04_N110_H40_R20_P100,100 (S4), incorporate no-fly zones to add layers of complexity to the planning task. In S3, the environment comprises 80 buildings and a larger no-fly zone (radius 40), evaluating the UAV's ability to plan longer detours around expansive restricted areas—a feature that is particularly beneficial in applications such as search and rescue in semi-rural outskirts [53], where UAVs have been used to quickly locate missing individuals. In contrast, S4 features 110 buildings and a smaller no-fly zone (radius 20), which is well suited for infrastructure inspection tasks, such as power line patrols or the autonomous circling of cell towers, as demonstrated by Li

et al. [54] and various pilot projects. Furthermore, these suburban scenarios are also applicable to environmental monitoring: UAVs can execute optimized, grid-based flight paths to cover agricultural fields for precision fertilization [55].

These suburban environment generated by the framework are designed to capture the transitional characteristics between urban and rural settings. Here, multiple sinusoidal components combined with Gaussian functions produce gentle rolling hills and moderate slopes, which are typical of suburban terrains. The building distribution is sparser compared to urban areas, with lower structures that still introduce various obstacles. This setup challenges UAVs to maneuver through gradually undulating landscapes while maintaining safe distances from sporadically placed obstacles, all under a slightly relaxed but still significant set of regulatory constraints. Such a representation mirrors the operational conditions that drones often face in suburban regions, where the balance between energy efficiency and obstacle avoidance becomes critical [56].

4.3. Mountainous

For the mountainous environment, six test cases have been carefully developed to examine the performance of UAV path planning algorithms in terrains characterized by rugged, uneven elevations and varying constraints, as depicted in Fig. 7. The first two cases, M01_N100_H300 (M1) and M02_N200_H300 (M2), focus on terrain variations created by the density of peaks. M1 features 100 peaks, resulting in a landscape with more isolated, prominent mountains, while M2 doubles the number of peaks to 200, creating a terrain reminiscent of a continuous mountain range. These variations allow for testing UAV algorithms in environments that challenge both path optimization around distinct obstacles and navigation through tightly grouped features—conditions that are representative of real-world mountainous regions. Such settings are particularly well suited for surveillance applications; for example, UAVs have been employed in terrain mapping and

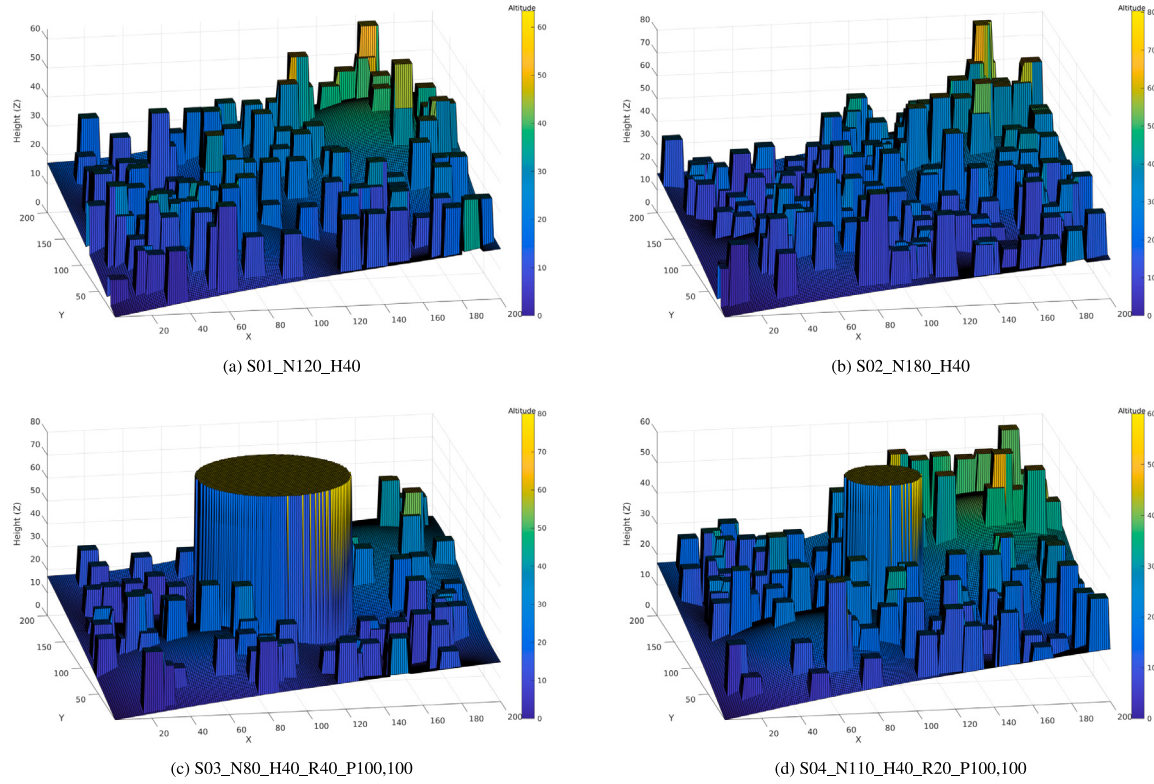


Fig. 6. Depictions of suburban test cases featuring moderate building densities, rolling terrain, and strategically placed no-fly zones. These scenarios reflect real-world challenges in suburban UAV navigation, balancing obstacle avoidance and efficiency.

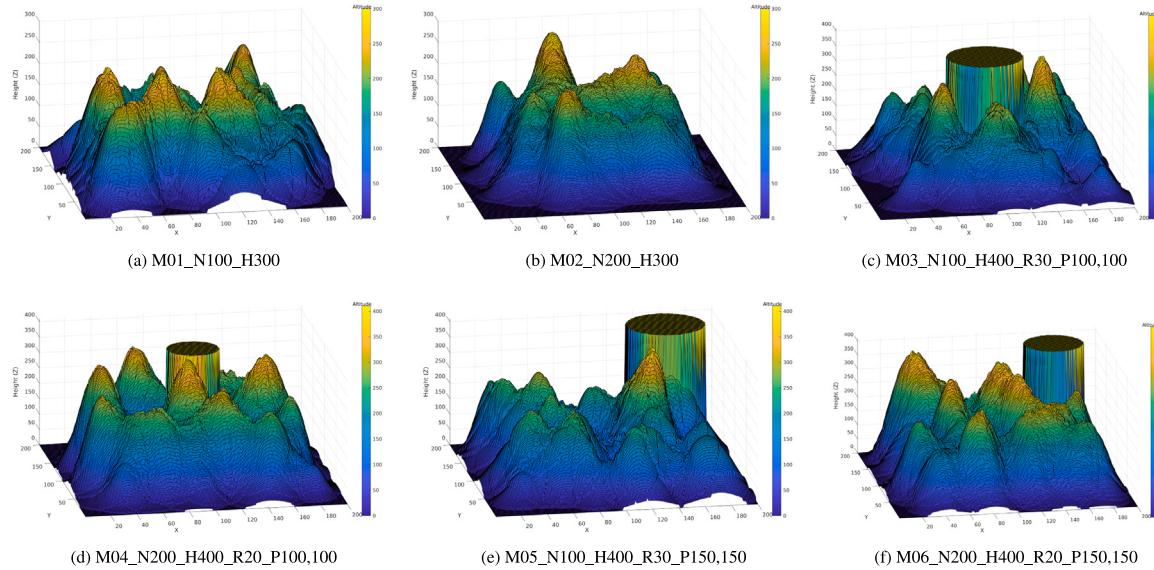


Fig. 7. Visualizations of mountainous test cases with varying peak densities, elevations, and no-fly zone configurations. These scenarios highlight the complexity of UAV navigation in rugged terrains, requiring robust path-planning strategies to handle steep gradients and restricted areas.

surveillance in mountainous forest regions [57,58], and in border security operations where drones monitor mountain ridge-lines to mitigate unauthorized crossings [59].

The next two cases incorporate no-fly zones to introduce additional constraints and challenges. These test environments: M03_N100_H400_R30_P100,100 (M3) and M04_N200_H400_R20_P100,100 represent terrains with increased peak heights (400 units) and varying no-fly zone radii. M3, with a sparser peak layout and a no-fly zone radius of 30 centered at (100, 100), tests the UAV's ability to plan paths around larger restricted areas while navigating prominent peaks. In

contrast, M4 includes a denser arrangement of 200 peaks and a smaller no-fly zone radius of 20, presenting a scenario that requires precise maneuvering through closely grouped mountains while avoiding restricted zones. These cases are especially relevant for logistics applications as shown by Shao et al. [60], Fischer et al. [61] and Choi et al. [62].

Two additional cases, M05_N100_H400_R30_P150,150 (M5) and M06_N200_H400_R20_P150,150 shift the no-fly zone center closer to the destination at (200, 200), introducing a unique challenge by placing the restricted region directly in the UAV's likely path. M5, with a sparser peak layout and a 30-unit no-fly zone, and M6, with

Table 2

Parameters for the 14 test environments used in the proposed benchmark. Each environment is characterized by distinct attributes such as terrain type, number of peaks or buildings, and no-fly zone specifications, enabling comprehensive evaluations across diverse UAV path-planning scenarios.

Problem name	Environment	Problem ID	$N_{\text{peaks}}/N_{\text{bldg}}$	$h_{\text{max}}^{\text{peaks}}/h_{\text{max}}^{\text{bldg}}$	h_{NFZ}	p_{NFZ}
C01_N100_H450	City	C1	100	450	—	—
C02_N150_H450	City	C2	150	450	—	—
C03_N100_H450_R20_P100,100	City	C3	100	450	20	(100, 100)
C04_N70_H450_R40_P100,100	City	C4	70	450	40	(100, 100)
S01_N120_H40	Suburban	S1	120	40	—	—
S02_N180_H40	Suburban	S2	180	40	—	—
S03_N80_H40_R40_P100,100	Suburban	S3	80	40	40	(100, 100)
S04_N110_H40_R20_P100,100	Suburban	S4	110	40	20	(100, 100)
M01_N100_H300	Mountainous	M1	100	300	—	—
M02_N200_H300	Mountainous	M2	200	300	—	—
M03_N100_H400_R30_P100,100	Mountainous	M3	100	400	30	(100, 100)
M04_N200_H400_R20_P100,100	Mountainous	M4	200	400	20	(100, 100)
M05_N100_H400_R30_P150,150	Mountainous	M5	100	400	30	(150, 150)
M06_N200_H400_R20_P150,150	Mountainous	M6	200	400	20	(150, 150)

a denser peak layout and a 20-unit no-fly zone, are designed to test the UAV's ability to handle dense and tightly constrained environments near critical waypoints. These scenarios are particularly suitable for search and rescue (SAR) operations [63,64], where real incidents have demonstrated the life-saving potential of carefully pre-planned UAV routes—as well as for infrastructure inspection tasks, such as the autonomous monitoring of power lines, pipelines, and dams in mountainous regions [65,66]. Additionally, these test cases support environmental monitoring applications; for example, UAVs have been used to detect early signs of wildfire through risk-weighted patrol paths and to conduct wildlife and ecology surveys over challenging mountainous terrain [67–69].

In these mountainous scenarios, the environment is generated to reflect the rugged and highly variable conditions of real-world high-altitude terrains. By combining a larger number of sinusoidal components with multiple Gaussian functions and adding random noise, the model creates steep gradients, pronounced peaks, and deep valleys that closely resemble the irregularities of natural landscapes, including rock formations and dense vegetation. Additionally, the strategic placement of no-fly zones simulates restricted airspace near high-elevation peaks, imposing significant operational constraints on UAV path planning. These features force algorithms to address rapid elevation changes and narrow safe corridors—challenges that are critical for drones operating in mountainous regions [70].

5. Experimental study

This section outlines the experimental design for benchmarking UAV path planning algorithms, incorporating a diverse set of state-of-the-art multi-objective optimization techniques. The algorithms under consideration span multiple paradigms to ensure a comprehensive evaluation. Among the Pareto-based methods, NSGA-II [28] employs non-dominated sorting and a crowding distance mechanism to maintain diversity along the Pareto front, while NSGA-II/SDR [71] enhances this approach using shift-based density estimation, making it more effective for irregularly distributed solutions. The decomposition-based algorithms, MOEA/D [72] and MOEA/D-AWA [73], transform multi-objective problems into scalar sub-problems, with MOEA/D focusing on uniform decomposition and MOEA/D-AWA introducing adaptive weight adjustment for dynamic problem landscapes. Indicator-based approaches include Hype [74], which prioritizes hypervolume maximization during selection, and I_{SDE+} [75], which leverages an advanced diversity indicator to achieve well-distributed Pareto solutions across multi- and many-objective scenarios. Additionally, MOEA-2DE [17], a recently proposed algorithm specifically tailored for UAV path planning, incorporates dimension exploration and discrepancy evolution to address domain-specific challenges such as dynamic obstacles, terrain non-linearity, and energy constraints. MOEA-2DE has

demonstrated superior performance in recent studies, making it a critical inclusion in this benchmarking exercise. This selection of algorithms allows the evaluation to capture performance nuances across Pareto-based, decomposition-based, indicator-based, and problem-specific strategies, providing a holistic view of algorithmic effectiveness for UAV path planning tasks. All algorithms were executed on the test environments (see Table 2) using a population size of 20 — selected to facilitate reproducibility — for a total of 10,000 function evaluations. Each experiment was independently repeated 30 times to ensure statistical reliability.

5.1. Performance metric

The performance of the algorithms was evaluated using the hypervolume (HV) metric, a widely regarded comprehensive indicator of multi-objective optimization performance. Hypervolume simultaneously captures two critical aspects of algorithm performance: convergence to the Pareto front and diversity of the solutions. Formally, hypervolume measures the volume of the objective space dominated by the solutions in the Pareto front, relative to a predefined reference point. It is defined as:

$$HV = \text{vol} \left(\bigcup_{x \in P} \{y \in \mathbb{R}^m | x \leq y \leq r\} \right), \quad (24)$$

where P is the set of Pareto-optimal solutions, m represents the number of objectives, and r is the reference point. A higher hypervolume indicates better performance, as it reflects both the proximity of solutions to the true Pareto front (convergence) and their spread across the objective space (diversity).

This dual characteristic renders hypervolume a suitable metric for evaluating algorithm effectiveness in the UAV path planning domain, eliminating the need for additional metrics like pure diversity. Metrics such as pure diversity explicitly focus on the spread of solutions without accounting for convergence. While this may provide additional insights in specific scenarios, it becomes redundant when using hypervolume, which already balances these two aspects in a single scalar value. Furthermore, pure diversity can penalize algorithms that prioritize convergence, potentially leading to misleading results [76]. Hypervolume, by contrast, avoids such biases by inherently rewarding both well-converged and well-distributed solutions. By relying solely on hypervolume, this evaluation aligns with the ultimate goal of multi-objective optimization: producing a well-converged and well-distributed Pareto front.

Given a problem, the reference point was chosen by examining the objective values obtained by all the algorithms and selecting a point that is significantly dominated by all observed solutions. The reference point was chosen to be significantly dominated by all observed solutions, thereby ensuring that it is worse than the worst objective

Table 3

Hypervolume metrics, including mean, standard deviation, and results from Wilcoxon signed-rank tests, for evaluating UAV path-planning algorithms across diverse test cases. The best performing results are represented in bold text.

Problem	NSGA-II	NSGA-II/SDR	MOEA/D	MOEA/D-AWA	HypE	I_{SDE+}	MOEA-2DE
C1	8.8041e - 01(5.5287e - 03) -	8.8097e - 01(7.2589e - 03) =	8.8243e - 01(8.5227e - 03) =	8.8558e - 01 (1.0149e - 02) +	8.8038e - 01(7.1695e - 03) =	8.7641e - 01(9.7313e - 03) -	8.5616e - 01(1.3064e - 02) -
C2	8.4381e - 01(1.4805e - 02) =	8.4843e - 01(1.6367e - 02) =	8.4129e - 01(1.1783e - 02) -	8.5152e - 01 (1.9031e - 02) +	8.4895e - 01(1.8355e - 02) =	8.3927e - 01(1.1097e - 02) -	8.1912e - 01(1.3804e - 02) -
C3	8.8356e - 01(1.4117e - 02) -	8.8054e - 01(1.6756e - 02) -	8.9330e - 01(5.0808e - 03) =	8.9489e - 01 (6.9459e - 03) +	8.8364e - 01(1.2828e - 02) -	8.7524e - 01(1.7406e - 02) -	8.4748e - 01(1.2228e - 02) -
C4	8.7100e - 01(1.5457e - 02) -	8.7349e - 01(2.0487e - 02) =	8.8100e - 01(1.2171e - 02) =	8.8336e - 01 (1.4016e - 02) +	8.6554e - 01(1.5094e - 02) -	8.5929e - 01(1.6846e - 02) -	8.4056e - 01(1.1247e - 02) -
S1	9.2688e - 01(1.7580e - 03) =	9.2630e - 01(1.8545e - 03) -	9.2612e - 01(1.2170e - 03) -	9.2714e - 01 (1.2274e - 03) +	9.2633e - 01(1.5653e - 03) -	9.2607e - 01(2.0795e - 03) -	9.2443e - 01(8.8858e - 04) -
S2	9.2266e - 01 (4.1152e - 03) +	9.2170e - 01(3.5228e - 03) -	9.1917e - 01(1.6877e - 03) -	9.2106e - 01(2.2293e - 03) =	9.2020e - 01(1.4611e - 03) -	9.1972e - 01(1.5736e - 03) -	9.1803e - 01(1.9096e - 03) -
S3	9.2213e - 01(1.4741e - 03) =	9.2231e - 01 (1.2729e - 03) +	9.2062e - 01(1.4628e - 03) -	9.2214e - 01(1.5479e - 03) =	9.2202e - 01(1.3217e - 03) =	9.2176e - 01(1.5070e - 03) =	9.2022e - 01(1.2044e - 03) -
S4	9.2251e - 01(1.6168e - 03) -	9.2374e - 01(1.7996e - 03) =	9.2214e - 01(9.9688e - 04) -	9.2344e - 01(1.6696e - 03) =	9.2393e - 01 (1.3403e - 03) +	9.2246e - 01(1.5838e - 03) -	9.2167e - 01(1.0708e - 03) -
M1	8.6613e - 01(1.9842e - 02) =	8.7000e - 01 (2.8054e - 02) +	8.4858e - 01(8.1769e - 03) -	8.5980e - 01(1.8279e - 02) =	8.6281e - 01(2.3053e - 02) =	8.5586e - 01(1.3758e - 02) -	8.6143e - 01(1.9021e - 02) =
M2	8.4929e - 01(0.0092e - 03) -	8.5233e - 01(1.5048e - 02) -	8.5443e - 01(2.0145e - 02) -	8.6021e - 01(2.5826e - 02) -	8.4917e - 01(2.1068e - 03) -	8.4991e - 01(2.0669e - 02) -	8.8427e - 01 (1.1377e - 02) +
M3	8.8497e - 01(2.8291e - 02) =	8.8400e - 01(2.7326e - 02) -	8.8581e - 01(1.6919e - 02) -	8.9578e - 01 (1.6671e - 02) +	8.7603e - 01(2.5164e - 02) -	8.6161e - 01(2.5033e - 02) -	8.7511e - 01(6.6799e - 03) -
M4	8.2709e - 01(2.6321e - 02) =	8.2882e - 01 (2.6041e - 02) +	8.1811e - 01(1.2504e - 02) =	8.2699e - 01(1.4862e - 02) -	8.2256e - 01(2.8107e - 02) -	8.1198e - 01(2.3737e - 02) -	8.1255e - 01(1.9814e - 02) -
M5	8.6813e - 01(1.4181e - 02) =	8.5928e - 01(1.1790e - 02) -	8.5821e - 01(8.1581e - 03) -	8.7192e - 01 (1.8043e - 02) +	8.5472e - 01(1.1017e - 02) -	8.4966e - 01(1.1317e - 02) -	8.4870e - 01(6.3941e - 03) -
M6	8.3139e - 01(4.5118e - 02) =	8.3710e - 01(4.4315e - 02) =	8.1626e - 01(2.4508e - 02) -	8.3886e - 01 (3.8545e - 02) +	8.1940e - 01(3.9079e - 02) -	8.0390e - 01(2.0886e - 02) -	8.2365e - 01(1.5393e - 02) =
+/-/=	1/5/8	3/5/6	0/10/4	8/1/5	1/8/5	0/13/1	1/11/2

+ denotes that the associated MOEA is the best performing MOEA.

= denotes that the associated MOEA is statistically equal with the best performing MOEA.

- denotes that the associated MOEA is statistically inferior to the best-performing MOEA.

value encountered in each objective. This approach is consistent with established practices in multi-objective optimization [28,74], as it guarantees that every solution on the Pareto front dominates the reference point, thereby providing a meaningful measure of the hypervolume. Regarding alternative metrics such as the Inverted Generational Distance (IGD), this metric measures the average Euclidean distance from points on the true Pareto front to the solutions obtained by an algorithm, thus reflecting both convergence and diversity. However, calculating IGD requires explicit knowledge of the true Pareto front [77]. While such true Pareto fronts are typically available for synthetic benchmark problems (e.g., CEC benchmarks), they are not known in the problem sets considered here, as our problems simulate real-world UAV path planning scenarios. As the true Pareto front is unknown, the IGD metric was deemed unsuitable for this evaluation.

6. Results and discussions

This section presents the results of the benchmark evaluation conducted to assess the performance of seven MOEAs across a diverse suite of UAV path-planning problems. The results are analyzed using the hypervolume metric, Wilcoxon signed rank statistical tests, convergence behavior, Pareto front distributions, and path visualizations. Additional detailed analyses, including Pareto fronts for all problems, convergence plots, and path visualizations, are provided in the supplementary material.

The hypervolume (HV) results, summarized in [Table 3](#), report the mean and standard deviation of HV values obtained over 30 independent runs for each algorithm. The Wilcoxon signed rank test, conducted at a significance level of 0.05, evaluates the statistical significance of differences between each algorithm and the best-performing algorithm for each problem. MOEA/D-AWA achieves the highest mean HV values in 8 out of 14 problems, demonstrating its effectiveness in maintaining a balance between convergence and diversity in the optimization process. This performance is particularly pronounced in problems with complex decision spaces, such as C1 (*dense urban scenario*) and M4 (*mountainous terrain*), where its adaptive weight adjustment mechanism enables efficient decomposition and exploration of the Pareto-optimal front. NSGA-II/SDR, while not the best-performing algorithm overall, achieves competitive results across several problems, demonstrating its ability to maintain a diverse and well-distributed set of solutions. The crowding distance mechanism in NSGA-II/SDR ensures effective exploration and robust convergence in moderately complex problems, such as S3 (*suburban environment*) and M1 (*mixed terrain*). In contrast, MOEA-2DE and I_{SDE+} frequently underperform across the majority of test problems, as indicated by their statistically significant inferiority in

Table 4

Ranking results of the Friedman test for multi-objective optimization algorithms evaluated on the UAV path-planning benchmark suite.

Algorithms	Ranking	Score
NSGA-II	4.857	3
NSGA-II/SDR	5.285	2
MOEA/D	3.642	5
MOEA/D-AWA	6.142	1
HypE	4.000	4
I_{SDE+}	2.071	6
MOEA-2DE	2.000	7

[Table 3](#). These algorithms appear to lack the exploration-exploitation balance required for high-dimensional and rugged decision spaces, leading to limited Pareto front diversity and suboptimal HV values.

The global performance of the algorithms is further assessed using the Friedman test rankings in [Table 4](#). MOEA/D-AWA ranks first, further confirming its robustness across a diverse set of scenarios. NSGA-II/SDR secures the second rank, underscoring its adaptability across varying problem complexities. HypE, while ranking fourth, demonstrates a strong focus on hypervolume maximization, making it particularly effective in problems where diversity is prioritized over convergence speed. Decomposition-based algorithms, including MOEA/D and RVEA, rank lower overall due to their limited ability to generalize across problems. Their tendency to optimize specific weighted combinations of objectives rather than maintaining a balanced trade-off across the entire Pareto front is evident in their suboptimal performance in higher-dimensional problems.

Convergence behavior, depicted in [Fig. 8](#), provides further insights into algorithmic dynamics. MOEA/D-AWA exhibits rapid convergence to high-quality solutions in dense urban scenarios like C1, demonstrating its computational efficiency and suitability for real-time UAV operations. In comparison, HypE, although slower to converge, ultimately achieves competitive HV values reflecting its strength in preserving solution diversity. NSGA-II and NSGA-II/SDR maintain stable convergence patterns, particularly in suburban environments (e.g., S1), highlighting their robustness in moderately constrained scenarios. Conversely, MOEA-2DE and I_{SDE+} exhibit slower convergence rates and limited final HV values, revealing limitations in their search strategies for complex multi-objective landscapes.

Pareto front visualizations, as shown in [Fig. 9](#) for problem S2, further validate these observations. MOEA/D-AWA and NSGA-II/SDR generate well-distributed Pareto fronts with strong convergence towards optimal trade-offs. The solutions are well distributed across the

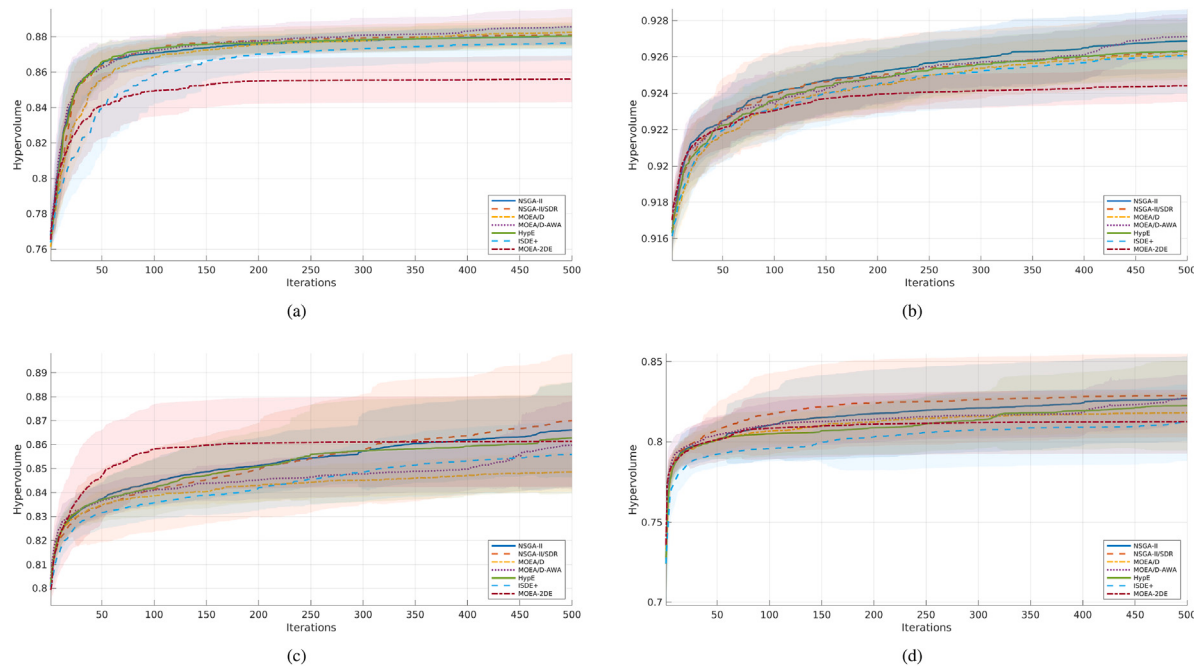


Fig. 8. Comparative analysis of algorithmic convergence trends for hypervolume metrics, averaged over 30 independent runs, showcasing performance dynamics in (a) Urban environment (C1), (b) Suburban environment (S1), (c) Mountainous environment with sparse peaks (M1), and (d) Mountainous environment with dense peaks and presence of NFZ (M4).

decision space, demonstrating effective exploration and exploitation. HypE, on the other hand, shows a tendency to cluster solutions at the extremes of the Pareto front, which aligns with its hypervolume-centric approach. MOEA-2DE and I_{SDE+} produce sparse, concentrated Pareto fronts, highlighting limited exploration capability for diverse trade-offs.

Path visualizations in Fig. 10 emphasize the practical implications of these findings. In urban environments like C1, MOEA/D-AWA and NSGA-II/SDR generate efficient paths that avoid obstacles while satisfying operational constraints, such as no-fly zones. In mountainous terrains like M4, MOEA/D-AWA produces paths with minimal altitude variation, demonstrating its capability to minimize energy consumption—a critical factor in UAV operations. In contrast, MOEA-2DE frequently generates paths with unnecessary detours, further explaining its lower HV rankings and reduced adaptability in complex environments.

In light of these overall trends, it is instructive to look more closely at the structural features and design philosophies of each algorithm, as this sheds light on why certain methods perform better under specific conditions. NSGA-II offers a robust, well-established framework based on non-dominated sorting and crowding distance, making it a compelling starting point for general UAV path-planning applications. Its primary strength is the ability to produce well-distributed Pareto fronts without extensive parameter tuning, which is beneficial when balancing flight distance and altitude constraints in moderately complex environments. By contrast, NSGA-II/SDR augments the crowding distance methodology with a shift-based density estimation approach, enhancing its ability to distribute solutions more evenly across an irregular or fragmented search space. In UAV applications where obstacles form complex corridors—such as mountainous areas with overlapping peaks; this emphasis on maintaining solution diversity becomes particularly valuable, as it broadens the range of feasible trade-offs between path length and safety margins.

MOEA/D, a decomposition-based framework, can be advantageous in settings where objectives are not only well defined but also exhibit relatively smooth variations. For instance, in suburban contexts where the terrain is mildly undulating and building density remains moderate, MOEA/D performs well by decomposing the multi-objective problem

into a set of simpler scalar subproblems. However, in highly constrained or irregular landscapes, researchers may find that careful tuning of weight vectors becomes necessary to retain adequate solution diversity. MOEA/D-AWA builds upon this decomposition principle by adaptively adjusting its subproblem weights as the search progresses, enabling dynamic adjustment of focus among competing objectives. This adaptive mechanism has exhibited strong performance in scenarios characterized by dense no-fly zones or abrupt altitude changes, as the algorithm is capable of quickly adjusting the decomposition vectors to explore underrepresented regions of the Pareto front. These features often translate to high hypervolume values in environments like cityscapes teeming with tall structures or mountain ranges where elevation varies sharply over short distances.

Indicator-based methods such as HypE, which prioritizes hypervolume contributions during selection, typically exhibit strengths in preserving a spread of well-distributed solutions. This advantage makes HypE suitable for early-stage mission planning or feasibility studies where the user might wish to explore a broad array of path options spanning extreme trade-offs (e.g., extremely low flight altitude vs. shortest path length). Nonetheless, HypE's focus on hypervolume increment can sometimes lead to slightly slower convergence rates in more complex UAV environments, particularly when faced with multiple high-dimensional constraints. Similarly, I_{SDE+} leverages an advanced diversity measure to distribute solutions more uniformly, rendering it useful in moderate-scale problems that do not present highly fractured or dynamic feasible spaces. Our results suggest, however, that in more convoluted or mountainous terrains, especially those featuring extensive no-fly zones, I_{SDE+} tends to struggle in identifying highly competitive solutions, necessitating further customization to maintain both diversity and convergence under more demanding conditions.

Finally, MOEA-2DE has been engineered with certain UAV-specific considerations, such as coping with dynamic constraints and terrain non-linearity. In missions where environments may change in near-real time (for instance, rapidly shifting meteorological conditions or minor obstacle relocations), MOEA-2DE's dimension-exploration strategies can enhance adaptability. While this can be advantageous for maintaining feasible flight corridors in more unpredictable situations,

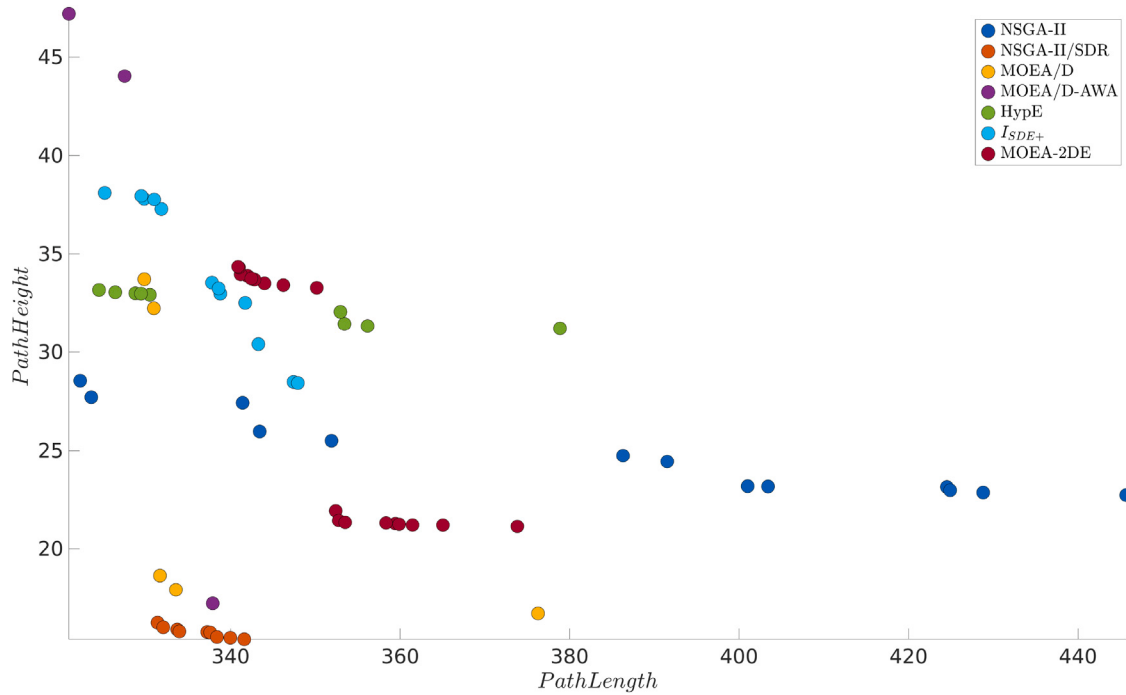


Fig. 9. Pareto front visualization for test problem S2 illustrating the trade-offs between objectives in a suburban environment.

our experiments suggest that MOEA-2DE may require additional parameter tuning to avoid superfluous exploration in relatively static environments. Taken together, these observations underscore the importance of matching the algorithmic design to the operational environment and mission objectives. In simpler contexts without significant altitude changes or unyielding no-fly zones, a classical method like NSGA-II may suffice and offer rapid deployment. In highly constrained or irregular terrains, either NSGA-II/SDR or MOEA/D-AWA will likely stand out due to their respective mechanisms for preserving diversity and adapting to dynamic search directions. Where research objectives involve thorough exploration of the objective space or complex, multi-dimensional constraints, indicator-based approaches such as HypE may yield broader coverage at the expense of slower convergence. Ultimately, by considering factors such as environment complexity, anticipated real-time changes, desired solution diversity, and ease of deployment, researchers can select the most suitable algorithm for their UAV path-planning tasks.

Collectively, these findings highlight distinct algorithmic trade-offs and confirm the critical role of aligning specific algorithmic strategies with particular environmental constraints and mission objectives. MOEA/D-AWA consistently excels in balancing convergence speed, diversity, and adaptability, emerging as the most robust algorithm across the evaluated scenarios. NSGA-II/SDR is a strong alternative for settings requiring high solution diversity and well-balanced trade-offs. Meanwhile, HypE preserves a wide spectrum of Pareto-optimal options at the cost of slower convergence, and both MOEA-2DE and I_{SDE+} show promise in specialized or smaller-scale problems but face adaptability challenges in more rugged landscapes. The supplementary material provides additional Pareto front plots, convergence behaviors, and path visualizations for all problems, further substantiating these conclusions and offering a detailed resource for future research in UAV path planning.

7. Conclusion and future works

This study introduced a benchmark for UAV path planning in complex environments, alongside a flexible framework for environment generation that supports the creation of custom scenarios with constraints such as altitude limits and no-fly zones. The 14 test problems presented here showcase the framework's capabilities and serve as a demonstration of its potential for broader applications. These problems highlight key challenges in UAV operations, including obstacle avoidance, regulatory constraints, and multi-objective trade-offs.

The performance of seven state-of-the-art MOEAs was evaluated using metrics such as hypervolume, Wilcoxon signed rank tests, convergence analysis, and Pareto front visualizations. MOEA/D-AWA consistently achieved superior results, balancing convergence and diversity across varied scenarios. NSGA-II/SDR demonstrated strong adaptability, particularly in moderately complex problems, while HypE preserved solution diversity at the cost of slower convergence. In contrast, decomposition-based algorithms showed limitations in generalizing to higher-dimensional and more intricate problem settings.

Beyond its role in academic benchmarking, the proposed framework can support a wide range of practical UAV applications. Example use cases include autonomous navigation for urban logistics (e.g., last-mile delivery and warehouse-to-consumer routing), environmental monitoring (e.g., forest surveillance and air-quality assessment), search and rescue operations in complex terrains, and infrastructure inspection (e.g., power lines, bridges, and building facades). The flexibility to simulate diverse environments and constraints makes the benchmark valuable for both algorithm development and pre-deployment validation.

Future work could extend the benchmark by incorporating dynamic constraints, such as temporally varying no-fly zones, and exploring scenarios with soft constraints alongside hard constraints. Additionally, integrating multi-agent coordination, real-time adaptability, and energy efficiency modeling would enhance the realism and versatility

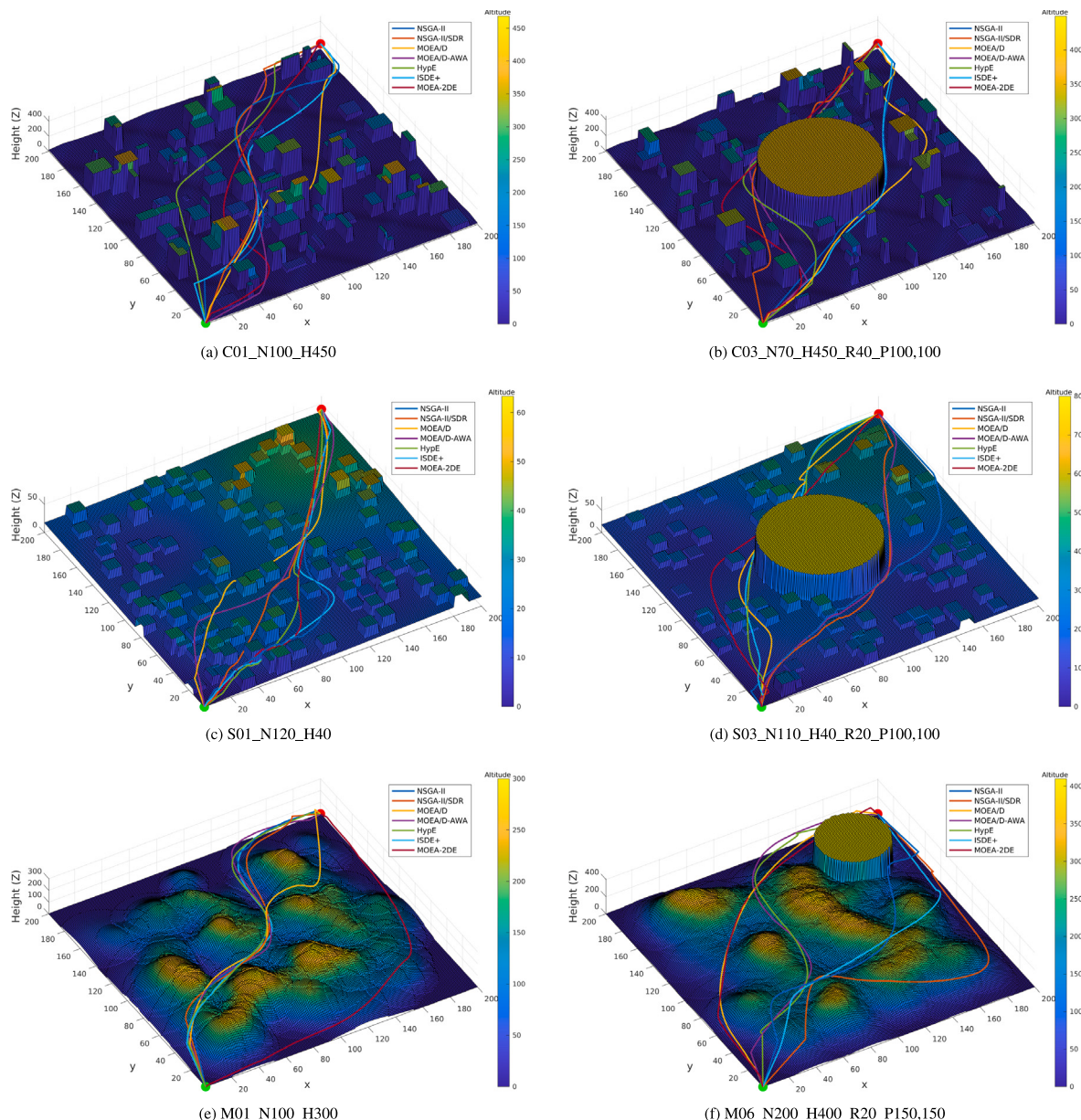


Fig. 10. Visualizations of paths generated by the baseline algorithms for the C1, C3, S1, S3, M1 and M4 environments. The starting and ending points for the path planning task are denoted using green and red dots respectively.

of the framework, supporting the development of more robust optimization algorithms for UAV path planning in real-world applications. Another promising direction involves shifting constraint handling from the problem formulation to the algorithm itself, enabling the algorithms to adaptively manage constraints. This approach could introduce greater flexibility and foster the development of constraint-aware optimization methods capable of addressing diverse and evolving problem settings.

Another potential enhancement involves in addressing a limitation of the current B-spline implementation. Presently, the B-spline path is validated by checking whether each control point intersects an obstacle and modifying the point accordingly to avoid it. However, there exist scenarios where, although the control points themselves do not lie within an obstacle, the interpolated curve between them may intersect with obstacles, resulting in impractical or unrealistic paths. Resolving this issue will involve enhancing the obstacle-avoidance mechanism to

account for intermediate path segments and ensuring the generated paths are fully viable in operational contexts.

CRediT authorship contribution statement

Daison Darlan: Writing – review & editing, Writing – original draft, Visualization, Software, Methodology, Investigation, Formal analysis, Data curation, Conceptualization. **Oladayo S. Ajani:** Writing – review & editing, Validation, Supervision, Investigation, Conceptualization. **Anand Paul:** Writing – review & editing, Validation, Resources, Project administration. **Rammohan Mallipeddi:** Writing – review & editing, Supervision, Resources, Project administration, Investigation, Conceptualization.

Declaration of competing interest

The authors hereby declare that there are no conflicts of interest related to the research, authorship, and/or publication of this article. No

financial or personal relationships exist that could have inappropriately influenced or biased the work presented in this manuscript.

Acknowledgments

This research was supported by the Core Research Institute Basic Science Research Program through the National Research Foundation of Korea(NRF) funded by the Ministry of Education Korea (2021R1A6A1A03043144).

Appendix A. Supplementary data

Supplementary material related to this article can be found online at <https://doi.org/10.1016/j.swevo.2025.101968>.

Data availability

The code and resources used in this study are publicly available at <https://github.com/Anomaly33/UAV-Path-Planning-Benchmark>. This repository includes implementations for environment generation, benchmark problem instances, and UAV path-planning algorithms.

References

- [1] X. Li, A.V. Savkin, Networked unmanned aerial vehicles for surveillance and monitoring: A survey, *Futur. Internet* 13 (7) (2021) 174.
- [2] A. Chriki, H. Touati, H. Snoussi, F. Kamoun, Uav-based surveillance system: an anomaly detection approach, in: 2020 IEEE Symposium on Computers and Communications, ISCC, IEEE, 2020, pp. 1–6.
- [3] M. Sajid, H. Mittal, S. Pare, M. Prasad, Routing and scheduling optimization for UAV assisted delivery system: A hybrid approach, *Appl. Soft Comput.* 126 (2022) 109225.
- [4] J. Li, H. Liu, K.K. Lai, B. Ram, Vehicle and UAV collaborative delivery path optimization model, *Mathematics* 10 (20) (2022) 3744.
- [5] S. Asadzadeh, W.J. de Oliveira, C.R. de Souza Filho, UAV-based remote sensing for the petroleum industry and environmental monitoring: State-of-the-art and perspectives, *J. Pet. Sci. Eng.* 208 (2022) 109633.
- [6] S. Ghambari, J. Lepagnot, L. Jourdan, L. Idoumghar, A comparative study of meta-heuristic algorithms for solving UAV path planning, in: 2018 IEEE Symposium Series on Computational Intelligence, SSCI, IEEE, 2018, pp. 174–181.
- [7] L. Rocha, K. Vivaldini, A 3d benchmark for uav path planning algorithms: Missions complexity, evaluation and performance, in: 2022 International Conference on Unmanned Aircraft Systems, ICUAS, IEEE, 2022, pp. 412–420.
- [8] D. Debnath, F. Vanegas, J. Sandino, A.F. Hawary, F. Gonzalez, A review of UAV path-planning algorithms and obstacle avoidance methods for remote sensing applications, *Remote. Sens.* 16 (21) (2024) 4019.
- [9] K. Danancier, D. Ruvio, I. Sung, P. Nielsen, Comparison of path planning algorithms for an unmanned aerial vehicle deployment under threats, *IFAC- Pap.* 52 (13) (2019) 1978–1983.
- [10] M. Popović, J. Ott, J. Rückin, M. Kochenderfer, Robotic Learning for Informative Path Planning. Available At SSRN 4798912.
- [11] S. Aggarwal, N. Kumar, Path planning techniques for unmanned aerial vehicles: A review, solutions, and challenges, *Comput. Commun.* 149 (2020) 270–299.
- [12] N. Hohmann, M. Bujny, J. Adamy, M. Olhofer, Multi-objective 3D path planning for UAVS in large-scale urban scenarios, in: 2022 IEEE Congress on Evolutionary Computation, CEC, IEEE, 2022, pp. 1–8.
- [13] N. Hohmann, S. Brulin, J. Adamy, M. Olhofer, Three-dimensional urban path planning for aerial vehicles regarding many objectives, *IEEE Open J. Intell. Transp. Syst.* (2023).
- [14] S. Primatesa, A 2.5 D risk-aware path planning method for safe UAS operations in populated environments, in: 2024 International Conference on Unmanned Aircraft Systems, ICUAS, IEEE, 2024, pp. 865–872.
- [15] S. Ghambari, M. Golabi, L. Jourdan, J. Lepagnot, L. Idoumghar, UAV path planning techniques: a survey, *RAIRO- Oper. Res.* 58 (4) (2024) 2951–2989.
- [16] M. Gao, X. Xu, Y. Klinger, J. Van Der Woerd, P. Tapponnier, High-resolution mapping based on an Unmanned Aerial Vehicle (UAV) to capture paleoseismic offsets along the Altyn-Tagh fault, China, *Sci. Rep.* 7 (1) (2017) 8281.
- [17] X. Xu, C. Xie, Z. Luo, C. Zhang, T. Zhang, A multi-objective evolutionary algorithm based on dimension exploration and discrepancy evolution for UAV path planning problem, *Inform. Sci.* 657 (2024) 119977.
- [18] C. Peng, S. Qiu, A decomposition-based constrained multi-objective evolutionary algorithm with a local infeasibility utilization mechanism for UAV path planning, *Appl. Soft Comput.* 118 (2022) 108495.
- [19] Y. Wan, Y. Zhong, A. Ma, L. Zhang, An accurate UAV 3-D path planning method for disaster emergency response based on an improved multiobjective swarm intelligence algorithm, *IEEE Trans. Cybern.* 53 (4) (2022) 2658–2671.
- [20] T. Quadt, R. Lindelauf, M. Voskuil, H. Monsuur, B. Čule, Dealing with multiple optimization objectives for UAV path planning in hostile environments: A literature review., *Drones* (2504- 446X) 8 (12) (2024).
- [21] G. Gugan, A. Haque, Path planning for autonomous drones: Challenges and future directions, *Drones* 7 (3) (2023) 169.
- [22] J. Luo, Y. Tian, Z. Wang, Research on unmanned aerial vehicle path planning, *Drones* 8 (2) (2024) 51.
- [23] R. Perez-Segui, P. Arias-Perez, J. Melero-Deza, M. Fernandez-Cortizas, D. Perez-Saura, P. Campoy, Bridging the gap between simulation and real autonomous uav flights in industrial applications, *Aerospace* 10 (9) (2023) 814.
- [24] M. Jones, S. Djahel, K. Welsh, Path-planning for unmanned aerial vehicles with environment complexity considerations: A survey, *ACM Comput. Surv.* 55 (11) (2023) 1–39.
- [25] A. Ait Saadi, A. Soukane, Y. Meraihi, A. Benmessaoud Gabis, S. Mirjalil, A. Ramdane-Cherif, UAV path planning using optimization approaches: A survey, *Arch. Comput. Methods Eng.* 29 (6) (2022) 4233–4284.
- [26] Q. Ren, Y. Yao, G. Yang, X. Zhou, Multi-objective path planning for UAV in the urban environment based on CDNSGA-II, in: 2019 IEEE International Conference on Service-Oriented System Engineering, SOSE, IEEE, 2019, pp. 350–3505.
- [27] K. Li, X. Yan, Y. Han, F. Ge, Y. Jiang, Many-objective optimization based path planning of multiple UAVs in oilfield inspection, *Appl. Intell.* 52 (11) (2022) 12668–12683.
- [28] K. Deb, A. Pratap, S. Agarwal, T. Meyarivan, A fast and elitist multiobjective genetic algorithm: NSGA-II, *IEEE Trans. Evol. Comput.* 6 (2) (2002) 182–197.
- [29] N. Wen, X. Su, P. Ma, L. Zhao, Y. Zhang, Online UAV path planning in uncertain and hostile environments, *Int. J. Mach. Learn. Cybern.* 8 (2017) 469–487.
- [30] N. Wen, L. Zhao, X. Su, P. Ma, UAV online path planning algorithm in a low altitude dangerous environment, *IEEE/ CAA J. Autom. Sin.* 2 (2) (2015) 173–185.
- [31] H. Qiu, H. Duan, A multi-objective pigeon-inspired optimization approach to UAV distributed flocking among obstacles, *Inform. Sci.* 509 (2020) 515–529.
- [32] X. Zhen, Z. Enze, C. Qingwei, Rotary unmanned aerial vehicles path planning in rough terrain based on multi-objective particle swarm optimization, *J. Syst. Eng. Electron.* 31 (1) (2020) 130–141.
- [33] Z. Yu, Z. Si, X. Li, D. Wang, H. Song, A novel hybrid particle swarm optimization algorithm for path planning of UAVs, *IEEE Internet Things J.* 9 (22) (2022) 22547–22558.
- [34] C. Qu, W. Gai, M. Zhong, J. Zhang, A novel reinforcement learning based grey wolf optimizer algorithm for unmanned aerial vehicles (UAVs) path planning, *Appl. Soft Comput.* 89 (2020) 106099.
- [35] X. Zhang, S. Xia, X. Li, T. Zhang, Multi-objective particle swarm optimization with multi-mode collaboration based on reinforcement learning for path planning of unmanned air vehicles, *Knowl.-Based Syst.* 250 (2022) 109075.
- [36] X. Hu, B. Pang, F. Dai, K.H. Low, Risk assessment model for UAV cost-effective path planning in urban environments, *IEEE Access* 8 (2020) 150162–150173.
- [37] R. Van Hoek, J. Ploeg, H. Nijmeijer, Cooperative driving of automated vehicles using B-splines for trajectory planning, *IEEE Trans. Intell. Veh.* 6 (3) (2021) 594–604.
- [38] A. Gasparetto, P. Boscaroli, A. Lanzutti, R. Vidoni, Path planning and trajectory planning algorithms: A general overview, *Motion Oper. Plan. Robot. Syst.: Backgr. Pr. Approaches* (2015) 3–27.
- [39] J.L. Foo, J. Knutzon, V. Kalivarapu, J. Oliver, E. Winer, Path planning of unmanned aerial vehicles using B-splines and particle swarm optimization, *J. Aerosp. Comput. Inf. Commun.* 6 (4) (2009) 271–290.
- [40] M.S. Hasan, M.N. Alam, M. Fayz-Al-Asad, N. Muhammad, C. Tunc, B-spline curve theory: An overview and applications in real life, *Nonlinear Eng.* 13 (1) (2024) 20240054.
- [41] T.A. Johansen, T.I. Fossen, Guidance, navigation, and control of fixed-wing unmanned aerial vehicles, in: M. Ang, O. Khatib, B. Siciliano (Eds.), *Encyclop Robotics*, 2020, pp. 1–9.
- [42] Y. Zhou, J. Shu, X. Zheng, H. Hao, H. Song, Real-time route planning of unmanned aerial vehicles based on improved soft actor-critic algorithm, *Front. Neurorobotics* 16 (2022) 1025817.
- [43] J. Muñoz, B. López, F. Quevedo, C.A. Monje, S. Garrido, L.E. Moreno, Multi UAV coverage path planning in urban environments, *Sensors* 21 (21) (2021) 7365.
- [44] B. Zhou, W. Liu, H. Yang, Unmanned aerial vehicle service network design for urban monitoring, *Transp. Res. Part C: Emerg. Technol.* 157 (2023) 104406.
- [45] M. Erdelj, E. Natalizio, K.R. Chowdhury, I.F. Akyildiz, Help from the sky: Leveraging UAVs for disaster management, *IEEE Pervasive Comput.* 16 (1) (2017) 24–32.
- [46] T. Chowdhury, M. Rahneemoonfar, R. Murphy, O. Fernandes, Comprehensive semantic segmentation on high resolution uav imagery for natural disaster damage assessment, in: 2020 IEEE International Conference on Big Data, Big Data, IEEE, 2020, pp. 3904–3913.
- [47] B.D. Song, K. Park, J. Kim, Persistent UAV delivery logistics: MILP formulation and efficient heuristic, *Comput. Ind. Eng.* 120 (2018) 418–428.
- [48] J. Kim, H. Moon, H. Jung, Drone-based parcel delivery using the rooftops of city buildings: Model and solution, *Appl. Sci.* 10 (12) (2020) 4362.

- [49] Z. Zheng, M. Pan, W. Pan, Virtual prototyping-based path planning of unmanned aerial vehicles for building exterior inspection, in: ISARC. Proceedings of the International Symposium on Automation and Robotics in Construction, Vol. 37, IAARC Publications, 2020, pp. 16–23.
- [50] S. Tian, Y. Li, X. Zhang, L. Zheng, L. Cheng, W. She, W. Xie, Fast UAV path planning in urban environments based on three-step experience buffer sampling DDPG, *Digit. Commun. Netw.* 10 (4) (2024) 813–826.
- [51] M. Szczepański, Vision-based detection of low-emission sources in suburban areas using unmanned aerial vehicles, *Sensors* 23 (4) (2023) 2235.
- [52] V. Garg, S. Niranjan, V. Prybutok, T. Pohlen, D. Gligor, Drones in last-mile delivery: A systematic review on efficiency, accessibility, and sustainability, *Transp. Res. Part D: Transp. Environ.* 123 (2023) 103831.
- [53] M. Lyu, Y. Zhao, C. Huang, H. Huang, Unmanned aerial vehicles for search and rescue: A survey, *Remote. Sens.* 15 (13) (2023) 3266.
- [54] Y. Li, X. Dong, Q. Ding, Y. Xiong, H. Liao, T. Wang, Improved A-STAR algorithm for power line inspection UAV path planning, *Energies* 17 (21) (2024) 5364.
- [55] J. Li, W. Zhang, J. Ren, W. Yu, G. Wang, P. Ding, J. Wang, X. Zhang, A multi-area task path-planning algorithm for agricultural drones based on improved double deep Q-learning net, *Agriculture* 14 (8) (2024) 1294.
- [56] D. Dobrilovic, Uav route planning in urban and suburban surveillance scenarios, in: Security-Related Advanced Technologies in Critical Infrastructure Protection: Theoretical and Practical Approach, Springer, 2022, pp. 217–227.
- [57] W. Wang, X. Li, J. Tian, UAV formation path planning for mountainous forest terrain utilizing an artificial rabbit optimizer incorporating reinforcement learning and thermal conduction search strategies, *Adv. Eng. Inform.* 62 (2024) 102947.
- [58] C.H. Singh, V. Mishra, K. Jain, High-resolution mapping of forested hills using real-time UAV terrain following, *ISPRS Ann. Photogramm. Remote. Sens. Spat. Inf. Sci.* 10 (2023) 665–671.
- [59] W. Wang, B. Jiang, J. Yang, C. Li, Research on UAV application in mountain anti-terrorism combat, in: Journal of Physics: Conference Series, Vol. 1792, (1) IOP Publishing, 2021, 012079.
- [60] P. Shao, C. Lin, K. Tsai, UAS medical delivery in rural/mountain areas under UTM surveillance, in: 2022 Integrated Communication, Navigation and Surveillance Conference, ICNS, IEEE, 2022, pp. 1–10.
- [61] P. Fischer, U. Rohrer, P. Nürberger, M. Manninger, D. Scherr, D. von Lewinski, A. Zirlik, C. Wankmüller, E. Kolesnik, Automated external defibrillator delivery by drone in mountainous regions to support basic life support—A simulation study, *Resusc. Plus* 14 (2023) 100384.
- [62] D.S. Choi, K.J. Hong, S.D. Shin, C.-G. Lee, T.H. Kim, Y. Cho, K.J. Song, Y.S. Ro, J.H. Park, K.H. Kim, Effect of topography and weather on delivery of automatic electrical defibrillator by drone for out-of-hospital cardiac arrest, *Sci. Rep.* 11 (1) (2021) 24195.
- [63] C. Vincent-Lambert, A. Pretorius, B. Van Tonder, Use of unmanned aerial vehicles in wilderness search and rescue operations: A scoping review, *Wilderness Environ. Med.* 34 (4) (2023) 580–588.
- [64] Y. Karaca, M. Cicek, O. Tatlı, A. Sahin, S. Paslı, M.F. Beser, S. Turedi, The potential use of unmanned aircraft systems (drones) in mountain search and rescue operations, *Am. J. Emerg. Med.* 36 (4) (2018) 583–588.
- [65] W.W. Greenwood, J.P. Lynch, D. Zekkos, Applications of UAVs in civil infrastructure, *J. Infrastruct. Syst.* 25 (2) (2019) 04019002.
- [66] Y. He, Z. Liu, Y. Guo, Q. Zhu, Y. Fang, Y. Yin, Y. Wang, B. Zhang, Z. Liu, UAV based sensing and imaging technologies for power system detection, monitoring and inspection: a review, *Nondestruct. Test. Eval.* (2024) 1–68.
- [67] S. Sudhakar, V. Vijayakumar, C.S. Kumar, V. Priya, L. Ravi, V. Subramaniyaswamy, Unmanned aerial vehicle (UAV) based forest fire detection and monitoring for reducing false alarms in forest-fires, *Comput. Commun.* 149 (2020) 1–16.
- [68] T. Yang, S. Zhang, Y. Wang, J. Liu, Optimized deployment of unmanned aerial vehicles for wildfire detection and monitoring, 2021, arXiv preprint [arXiv:2112.03010](https://arxiv.org/abs/2112.03010).
- [69] J. Gonçalves, R. Henriques, P. Alves, R. Sousa-Silva, A.T. Monteiro, Â. Lomba, B. Marcos, J. Honrado, Evaluating an unmanned aerial vehicle-based approach for assessing habitat extent and condition in fine-scale early successional mountain mosaics, *Appl. Veg. Sci.* 19 (1) (2016) 132–146.
- [70] S. Wang, L. Zhang, L. Luo, Y. Zeng, A path planning method of UAV in mountainous environment, in: 2021 IEEE 5th Information Technology, Networking, Electronic and Automation Control Conference, ITNEC, Vol. 5, IEEE, 2021, pp. 1399–1404.
- [71] F. Yang, L. Xu, X. Chu, S. Wang, A new dominance relation based on convergence indicators and niching for many-objective optimization, *Appl. Intell.* (2021) 1–18.
- [72] Q. Zhang, H. Li, MOEA/D: A multiobjective evolutionary algorithm based on decomposition, *IEEE Trans. Evol. Comput.* 11 (6) (2007) 712–731.
- [73] Y. Qi, X. Ma, F. Liu, L. Jiao, J. Sun, J. Wu, MOEA/D with adaptive weight adjustment, *Evol. Comput.* 22 (2) (2014) 231–264.
- [74] J. Bader, E. Zitzler, HypE: An algorithm for fast hypervolume-based many-objective optimization, *Evol. Comput.* 19 (1) (2011) 45–76.
- [75] T. Pamulapati, R. Mallipeddi, P.N. Suganthan, ISDE+—an indicator for multi and many-objective optimization, *IEEE Trans. Evol. Comput.* 23 (2) (2018) 346–352.
- [76] H. Seada, M. Abouhawwash, K. Deb, Towards a better balance of diversity and convergence in NSGA-III: First results, in: Evolutionary Multi-Criterion Optimization: 9th International Conference, EMO 2017, Münster, Germany, March 19–22, 2017, Proceedings 9, Springer, 2017, pp. 545–559.
- [77] H. Ishibuchi, Y. Sakane, N. Tsukamoto, Y. Nojima, Evolutionary many-objective optimization by NSGA-II and MOEA/D with large populations, in: 2009 IEEE International Conference on Systems, Man and Cybernetics, IEEE, 2009, pp. 1758–1763.